Generation of ultrashort laser pulses using gas-filled hollow waveguides

Master Thesis
by
Johan Mauritsson

Lund Reports on Atomic Physics, LRAP-247
Lund, August 1999

Abstract

In this thesis work a new pulse compression technique has been implemented for the 110 fs, 10 Hz terawatt laser in Lund. The technique uses a gas-filled hollow waveguide to broaden the spectrum of the pulses and produce a linear chirp. This is achieved by the combined effects of self phase modulation and group velocity dispersion. After the pulses have passed through the hollow waveguide they are compressed in a compressor consisting of two prisms. A single shot autocorrelator was used to measure the time duration of the compressed pulses. Pulses with a time duration less than 50 fs were routinely produced with a best result of 13 fs pulses with 0.3 mJ per pulse.

Contents

1 Introduction

1.1 History

Ever since the invention of the laser in 1960 people have been trying to produce laser pulses with shorter and shorter time duration. There are several reasons for this, one is that the peak power is increased if the energy is not changed when the time duration is decreased. Another reason is that many phenomena in nature are very fast, for example chemical reactions, and to be able to measure these phenomena ultrashort laser pulses are needed.

There are two approaches to producing ultrashort laser pulses:

1. To improve the laser cavity so that the output laser pulses becomes shorter.
2. To compress the laser pulses once they are produced with some external device.

The combination of these two approaches has resulted in a very rapid decrease in the time duration over the years. In Figure 1 the shortest time duration is plotted as a function of time.

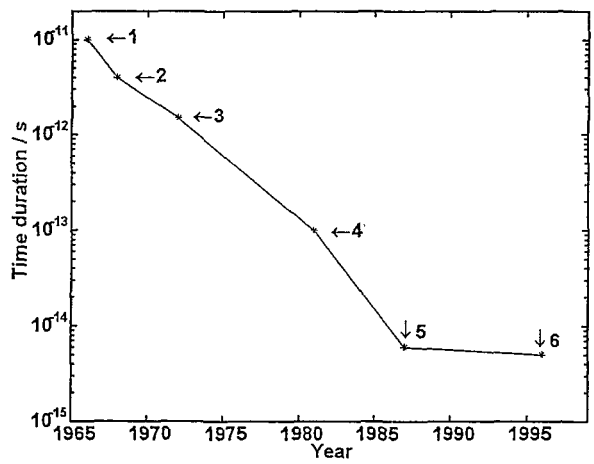

Figure 1. The shortest time duration as a function of time. The different points were found in: 1-4 [1], 5 [2] and 6 [3].

To decrease the time duration of the output laser pulses, different designs of the laser cavity have been invented. By using Q-switching, cavity dumping and mode locked lasers the time duration has decreased. A mode locked dye-laser gives the possibility of achieving a time duration below 100 fs ($1\ \text{fs} = 10^{-15}\ \text{s}$). Recently the development has been in favor of crystals instead of dyes since crystals are not toxic and easier to handle. The use of crystals for broad-band laser purposes was for a long time limited due to the

poor quality of the crystals. The fast development in solid state techniques has rapidly improved the quality and crystals are now widely used in lasers. The crystal capable of producing the shortest pulses today is sapphire doped with titanium, $Ti^{3+}:Al_2O_3$ which has been used to produce pulses shorter than 10 fs [4]. In theory it should be able to produce pulses shorter then 4 fs, due to the large gain bandwidth of $Ti^{3+}:Al_2O_3$. To get pulses this short directly from the laser is, however, very difficult. For this reason there is a need for an external device to compress the pulses.

In 1984 Tomlinson *et al.*, showed that it was possible to compress laser pulses using optical fibers and gratings [5]. This technique, however, is limited to pulses with very low energy, a few nJ, or else the material will be destroyed. In 1996 Svelto *et al.*, showed that it was possible to increase the energy if a gas-filled hollow waveguide (capillary) was used instead of the fiber [6]. This technique has later been improved to produce pulses shorter than 5 fs with energy about 0.5 mJ [7], which gives a power of 0.1 TW. These pulses were produced starting with 20 fs laser pulses with a repetition rate of 1 kHz.

1.2 The pulse compression technique in brief

The theory of how to compress the laser pulses is presented in the following chapters, and is dictated by the following rule: The time-bandwidth product of a pulse is greater than or equal to a constant. Therefore, to shorten the pulses the spectrum has to be broadened. The broadening of the spectrum can be achieved by using the fact that the refractive index of most transparent media is intensity-dependent. Since the intensity changes during a laser pulse different parts of the pulse experience different refractive index, this in turn leads to a *spectral broadening*. For the compressed pulses to have a good temporal shape this is not enough. The spectrum has to be broadened in such a way that it is possible to compress the pulses. The refractive index is also wavelength-dependent. Since short pulses cover a broad wavelength range they will experience different refractive index. This leads to a *temporal broadening* of the pulse since the long wavelength components travel with a higher speed than the short wavelength components in all natural materials. In Chapter 2 it will be explained how the above mentioned effects can be combined to produce a broadening of the spectrum in such way that the pulses are compressible.

To achieve the correct balance between the intensity- and the wavelength-dependence the cross section of the laser beam has to be quite small over a certain distance. This can be achieved by focusing the laser into a capillary. The capillary acts as a waveguide and will constrain the beam to a certain area. The waveguide properties of a capillary are not as good as in the case of optical fibers[1] and therefore the capillary cannot be too long and must be kept straight to minimize losses [8]. The advantage of a gas-filled capillary is that the pulse energy can be increased compared to maximum pulse

[1]Since the refractive index of the walls in the capillary is greater than the refractive index of the gas inside, there cannot be total reflection as in an optical fiber where the ratio is inverse.

energy possible to transmit through a fiber, since the material in the fiber is destroyed by too high intensity. The gas in the capillary, on the other hand, might be ionized but this occurs at a much higher intensity than the damage threshold of the fiber and the gas recovers before the next laser pulse, "self healing". The pressure and the gas composition affects the refractive index inside the capillary. Due to this the capillary has to be built into a system which can be evacuated and filled with the right gas to the optimum pressure. It is preferable to use inert gases since they do not form molecules. In molecular gases there are effects due to molecular rotations and vibrations that add to the electronic effects and the ionization threshold may be lower. The molecular motion is slow compared to the electronic response and some approximations used to simulate the propagation in the following chapters are no longer valid. This makes it difficult to understand how the pulses are affected and how they should be compressed. It might even result in pulses that are not compressible.

After the beam has passed the capillary it is collimated by a spherical mirror and guided into the compressor. The compressor used in this work is built up by the author of this thesis, using two prisms through which the pulses pass twice. In the compressor the short wavelength components travel faster than the long wavelength components and thus the pulses are compressed [9]. The pulses are finally sent to an autocorrelator where the pulse duration is measured.

1.3 The purpose of this master thesis

The purpose of this master thesis is to implement, at the terawatt laser in Lund, the pulse compression technique developed by Svelto *et al* . The Lund terawatt laser produces 110 fs long pulses with energies up to 300 mJ resulting in a peak-power of $\sim$ 3 TW. The repetition rate of the laser is 10 Hz. The goal has been to compress a small amount of the energy, $\sim$ 1 mJ, of the 110 fs long pulses to below 50 fs. The focus has been on decreasing the time duration and not to increase the peak power.

The time duration of ultrashort laser pulses is difficult to measure since the fastest electronic devices today, streak cameras, have a resolution of a few 100 fs. Instead the shortest available measurement scale has to be used, namely the pulse itself. A device that uses the pulse itself to measure the time duration is called an autocorrelator. A second goal for this master thesis was to build an autocorrelator to measure the compressed pulses.

The technique is later to be implemented on another system at the Lund High-power Laser Facility which produces 30 fs laser pulses at a repetition rate of 1 kHz with the aim of compressing them to less than 10 fs. These pulses will then be used to measure the time duration of the high-order harmonics produced at the Facility. The high-order harmonics have very short time duration and short wavelength. The short wavelength makes it difficult to use an autocorrelator to measure their time duration[2] and therefore

[2]The nonlinear process used in the autocorrelator is proportional to the wavelength and for short

cross correlation [10] with laser pulses of known, and very short, length is preferable. The cross correlation works approximately as the autocorrelator but here one pulse has a known time duration and one an unknown. When the two pulses intersect in a gas, two photon absorption is possible and measurable.

---

wavelength the signal will be very weak. For short wavelengths, in this case xuv, no crystals exist that are transparent.

2 The theory of pulse compression using hollow waveguides

2.1 The time-bandwidth product

For laser pulses there is a relation between the pulse duration and the spectral bandwidth. The product of the two is always less than or equal to some constant

$$\Delta\omega \cdot \Delta t \geq const. \tag{1}$$

The value of the constant depends on the shape of the pulse [11]. If the shape is Gaussian (e^{-t^2}) the constant equals $2\pi \cdot 0.441$ (the factor 2π is due to the fact that ω is the angular frequency, $\omega = 2\pi\nu$, where ν is the frequency). In most cases when pulse duration is studied the shape is instead assumed to be $\mathrm{sech}^2(t)$ since this is one solution to the equation describing the pulse shape in the laser cavity. In this case the constant equals $2\pi \cdot 0.315$ so that the result will be shorter pulses with the same bandwidth. A pulse where (1) is an equality is known as a transform limited pulse. For a transform limited pulse the temporal shape of the pulse is given by the Fourier transform of the spectrum[3].

Usually it is easier to consider the wavelength instead of the frequency. Using the following relations, and assuming transform limited pulses, equation (1) can be rewritten:

$$\omega = 2\pi\nu = \frac{2\pi c}{\lambda}, \tag{2}$$

$$\Delta\nu = \frac{c}{\lambda^2}\Delta\lambda, \tag{3}$$

$$\Longrightarrow \Delta\lambda = \frac{\lambda^2}{c}\frac{a}{\Delta t}. \tag{4}$$

Where $a = 0.441$ for a Gaussian and 0.315 for a sech^2 pulse shape. Equation (4) shows that a Gaussian pulse with central wavelength at 800 nm and a pulse duration of 110 fs have to have a bandwidth of at least $\Delta\lambda = 8.6$ nm. To compress the pulse to, say, 20 fs requires $\Delta\lambda$ to be increased to at least 47.1 nm.

2.2 Pulse propagation

Light can be described as an electromagnetic wave. In most cases it is just the effects of the electric field that is apparent and the magnetic field is left out in the description (since $\mu \simeq 1$ in insulators). However, it is always there and may in some cases be of importance. In this thesis the magnetic field will be left out since the studied effects all are due to the electric field. The propagation of a light pulse in a medium is described by the non-linear propagation equation: (derived in appendix A)

$$i\frac{\partial U}{\partial z} = \frac{sgn(\beta_2)}{2L_D}\frac{\partial^2 U}{\partial \tau^2} + i\frac{sgn(\beta_3)}{6L_D'}\frac{\partial^3 U}{\partial \tau^3} - \frac{e^{-\alpha z}}{L_{NL}}\left[|U|^2 U + is\frac{\partial}{\partial \tau}\left(|U|^2 U\right)\right]. \tag{5}$$

[3]This is how to calculate the time-bandwidth constant for different pulse shapes.

A normalized amplitude U and normalized time scale τ are used [12]:

$$\tau = \frac{T}{T_o} = \frac{t - \beta_1 z}{T_o}, \tag{6}$$

$$A(z,\tau) = \sqrt{P_o}\exp\left(-\frac{\alpha z}{2}\right)U(z,\tau), \tag{7}$$

where A is the slowly varying envelope of the pulse and T_o is the initial $1/e$ half width of the pulse. τ is a normalized time scale in the frame of reference of the pulse (it moves along with the pulse). The effect of each term on the pulse properties will be presented in the following subsections. As an overview, however, it can be said that the first term on the right hand side in equation (5) accounts for the broadening of the pulse due to group velocity dispersion, GVD. The second term accounts for broadening of the pulse due to third order dispersion, TOD, and $e^{-\alpha z}$ are the losses in the capillary. $\frac{1}{L_{NL}}|U|^2 U$ broadens the spectrum due to self phase modulation, SPM, and $\frac{is}{L_{NL}}\frac{\partial}{\partial\tau}\left(|U|^2 U\right)$ makes the temporal and spectral shape of the pulse asymmetric, due to self steepening.

To be able to see exactly how the pulse is affected by the medium, equation (5) has to be solved. However, to solve it is quite difficult and must be done numerically. If all terms but one are excluded the equation is possible to solve analytically and the effects of the remaining term can be studied. A feeling for how the different terms affects the pulse is important in order to understand their combined effect.

2.2.1 Group velocity dispersion, GVD

One way to describe a laser pulse is to say that the electric field is given by:

$$E(t,z) = \int_{-\infty}^{\infty} A_\omega(\omega - \omega_L)\exp\left[j(\omega t - \beta z)\right]d\omega, \tag{8}$$

where A_ω is the complex amplitude, $\beta = \frac{2\pi n(\omega)}{\lambda}$ is the wave number where $n(\omega)$ is the refractive index and ω_L is the central frequency [13]. The wave number β depends on the frequency and for pulses with quite narrow spectral width this dependency can be approximated with a linear approximation (Taylor expansion around ω_L)

$$\beta = \beta_L + \left(\frac{\partial\beta}{\partial\omega}\right)_{\omega_L}(\omega - \omega_L) + ..., \tag{9}$$

Substituting this relation into (8) gives the following expression for the electric field:

$$E(t,z) = \exp\left[j(\omega_L t - \beta_L z)\right]\cdot\int_{-\infty}^{\infty} A_\omega(\Delta\omega)\exp\left\{j\Delta\omega\left[t - \left(\frac{\partial\beta}{\partial\omega}\right)_{\omega_L} z\right]\right\}d\Delta\omega. \tag{10}$$

This equation can be rewritten as:

$$E(t,z) = A\left[t - \left(\frac{z}{v_g}\right)\right]\exp\left[j(\omega_L t - \beta_L z)\right], \tag{11}$$

where A is the pulse amplitude, $\exp\left[j\left(\omega_L t - \beta_L z\right)\right]$ is the carrier wave and v_g is the group velocity given by:

$$v_g = \left(\frac{\partial \omega}{\partial \beta}\right)_{\beta=\beta_L}. \tag{12}$$

The group velocity is the speed with which the pulse travels and it may be slower than the phase velocity which is the speed with which each wave travels. If the pulses are short the spectral width is quite broad and the linear approximation of the wave number is no longer a good approximation. Instead the next term in the Taylor expansion must be taken into account as well:

$$\beta = \beta_L + \left(\frac{\partial \beta}{\partial \omega}\right)_{\omega_L}(\omega - \omega_L) + \frac{1}{2}\left(\frac{\partial^2 \beta}{\partial \omega^2}\right)_{\omega_L}(\omega - \omega_L)^2 + ... \tag{13}$$

If $\left(\frac{\partial^2 \beta}{\partial \omega^2}\right)_{\omega_L}$ is non zero, the group velocity is different for different frequencies and the pulse will become temporally longer. The time separation between the fastest and slowest component of the pulse after travelling a distance l is given by:

$$\Delta\tau = \left(\frac{l}{v_g(1)} - \frac{l}{v_g(2)}\right) = l\left[\left(\frac{\partial \beta}{\partial \omega}\right)_{\omega_1} - \left(\frac{\partial \beta}{\partial \omega}\right)_{\omega_2}\right] \simeq l\left|\left(\frac{\partial^2 \beta}{\partial \omega^2}\right)_{\omega_L}\right| \Delta\omega_L. \tag{14}$$

This phenomena is known as group velocity dispersion, *GVD*. Depending on the sign of $\left(\frac{\partial^2 \beta}{\partial \omega^2}\right)_{\omega_L}$ (from now on called β_2) one talks about negative or positive dispersion. All normal materials have positive dispersion ($\beta_2 > 0$) which changes the pulses so that the leading edge of the pulse will have lower frequencies than the trailing edge, as depicted in Figure 2.

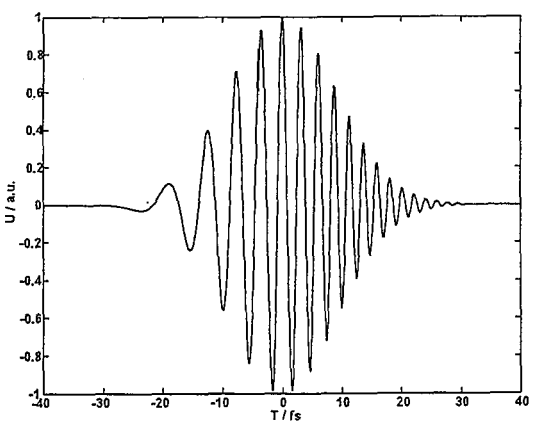

Figure 2. Exaggerated picture of the electric field of a pulse with positive chirp.

If GVD is the only thing that affects the pulse the frequency will change linearly. This is called a linear chirp. A linear chirp can be compensated for by introducing a device with negative GVD, for example a pair of gratings or a pair of prisms. Figure 2 shows an exaggerated picture of a pulse with a positive chirp. Notice that the left part of the

pulse is the leading edge. If equation (5) is solved with only the GVD term included, the resulting formula for the electric field becomes:

$$U(z,T) = \left(\frac{T_o^2}{T_o^2 - i\beta_2 z}\right)^{1/2} \exp\left(-\frac{T^2}{2\left(T_o^2 - i\beta z\right)}\right) \tag{15}$$

and the temporal width:

$$T_1 = T_o\sqrt{1 + \left(\frac{z}{L_D}\right)^2}. \tag{16}$$

Where L_D is the dispersion length given by $L_D = \frac{T_o^2}{|\beta_2|}$.

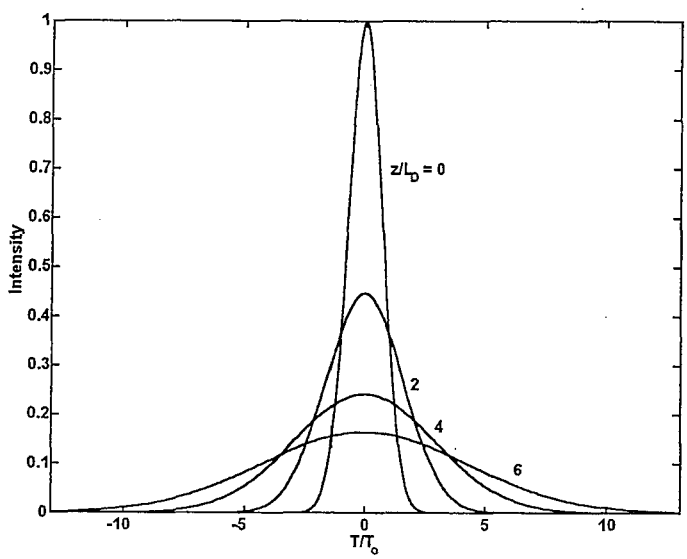

Figure 3. The pulse shape for different propagation distances $\frac{z}{L_D}$.

Figure 3 shows how the pulse shape changes when the pulses are only affected by GVD. The physical interpretation of L_D is that it is the distance a pulse has to travel in the material for its time duration to increase by a factor $\sqrt{2}$.

If the pulses are very short, more terms must be added in the Taylor expansion of β and these terms are known as higher order dispersion. This is presented in more detail in Chapter 2.2.4.

2.2.2 Self phase modulation, SPM

As mentioned before it is the fact that the refractive index is intensity dependent that makes the spectral broadening possible. With only third order susceptibility taken into account the refractive index can be written as:

$$n(t) = n_o + n_2 I(t). \tag{17}$$

This implies that also the phase, ϕ, will depend on the intensity and time

$$\phi = \omega_o t - \beta z = \omega_o t - \frac{\omega_o n_o z}{c} - \frac{\omega_o n_2 I(t) z}{c}, \tag{18}$$

and since the frequency is given by the time derivative of the phase [12], the frequency will also be intensity and time dependent:

$$\omega = \frac{\partial \phi}{\partial t} = \omega_o - \frac{\omega_o n_2}{c} \frac{\partial I}{\partial t} z. \tag{19}$$

This equation indicates that new frequencies will be created. For the leading edge of the pulse the frequency will shift towards red, since $\frac{\partial I}{\partial t} > 0$. The center of the pulse will not change since the derivative here is zero and the trailing edge will shift towards blue. It is convenient to introduce a new parameter called the non-linear length, $L_{NL} = \frac{1}{\gamma P_o}$ [12], where $\gamma = \frac{n_2 \omega_o}{c A_{eff}}$ is the nonlinearity coefficient, P_o is the peak power of the pulse and A_{eff} is the effective area of the pulse. The physical meaning of L_{NL} is that the maximum phase-shift, $\phi_{\max}$, is equal to 1 when the pulse has propagated this distance. If all effects but the SPM are neglected[4], equation (5) can be reduced to

$$\frac{\partial U}{\partial z} = \frac{i}{L_{NL}} \exp(\alpha z) |U|^2 U. \tag{20}$$

This equation can be solved analytically

$$U(z,T) = U(0,T) \exp[i \phi_{NL}(z,T)], \tag{21}$$

$$\phi_{NL} = |U(0,T)|^2 (z_{eff}/L_{NL}), \tag{22}$$

$$z_{eff} = \frac{1}{\alpha} [1 - \exp(-\alpha z)]. \tag{23}$$

If the losses, α, are neglected $z_{eff} = z$ and the maximum phase-shift is then given by

$$\phi_{\max} = \frac{z}{L_{NL}}. \tag{24}$$

The chirp of a Gaussian pulse after it has been modified by SPM is given by

$$\delta\omega(T) = \omega(T) - \omega_o = \frac{2}{T_o} \phi_{\max} \left(\frac{T_o}{T}\right) \exp\left[-\left(\frac{T}{T_o}\right)^2\right]. \tag{25}$$

[4] GVD can for example be neglected compared to SPM if $L_D >> L_{NL}$.

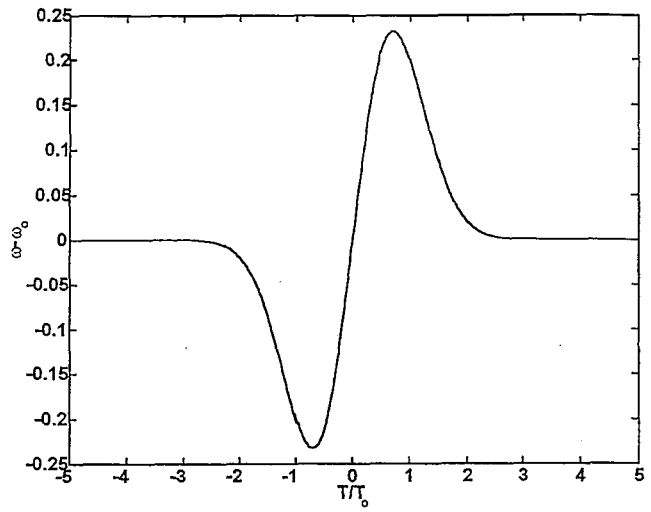

Figure 4. The chirp of a pulse only affected by SPM.

It is also possible to get the spectrum which is given by:

$$S(\omega) = \left| \int_{-\infty}^{\infty} U(0,T) \exp\left[i\phi_{NL}(z,T) + i(\omega - \omega_o)T \right] dT \right|^2 . \tag{26}$$

Depending on the value of $\phi_{\max}$ there will be a different number of peaks, M, in the spectrum approximated by, [12]:

$$\phi_{\max} = \left(M - \frac{1}{2} \right) \pi. \tag{27}$$

The chirp of a pulse affected by SPM is depicted if Figure 4 and the spectra of pulses for different value on $\phi_{\max}$ are presented in Figure 5.

In the case of pure SPM the chirp is not linear, which makes it impossible to compress the pulse as explained later. It is however possible to broaden the spectrum and at the same time make sure that the chirp will become linear. This is possible if SPM acts not alone but together with the group velocity dispersion. This is discussed in the following subsection.

2.2.3 The combined effect of SPM and GVD

Since SPM produces low frequency components in the first part of the pulse, and these components travel faster than the high frequency components due to GVD (and the other way around for the trailing edge), the combined effect of GVD and SPM will be that the pulse broadens faster than if GVD were to act alone.

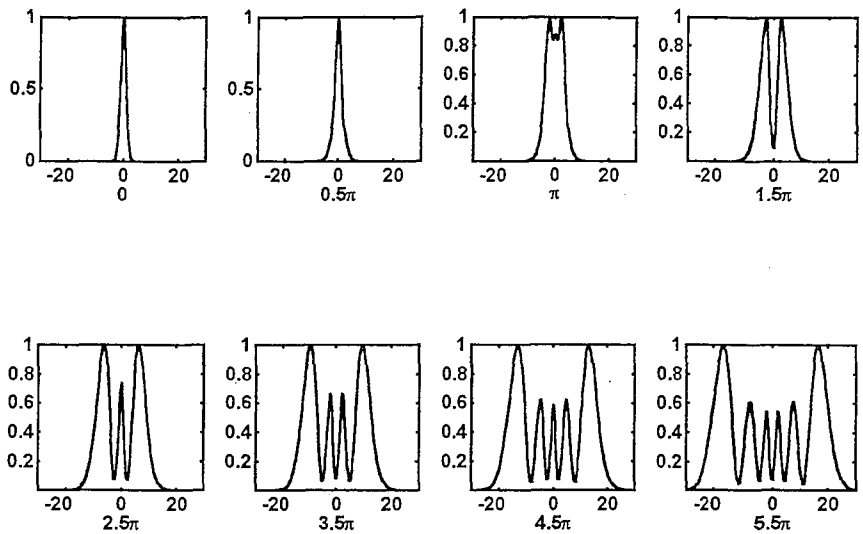

Figure 5. Calculated SPM-broadened spectra for different values on the maximum phase shift $\phi_{\max}$. The x-axes corresponds to the frequency and the y-axes to the normalized intensity.

The effect of SPM is greatest when the pulse slope is largest, that is in the beginning and the end. Therefore, the combined effect of GVD and SPM will also be greatest here, resulting in a stretching of the pulse in such a way that it more and more resembles a square pulse. Since the central parts of the pulse is almost flat, SPM does no longer contribute to this part. At the leading and trailing edges, on the other hand, the intensity changes rapidly and SPM results in new frequency components at these locations. This results in a chirp that is almost linear.

The combined effects of GVD and SPM will consequently lead to a broader spectrum and with a linear chirp. That is a pulse that is compressible to shorter pulse duration than the original pulse and still having a nice temporal shape (a nice temporal shape is smooth and without pre- and/or post-pulses). In Figure 6 the effect of SPM is compared to the combined effect of SPM and GVD. The comparisons are being made between the pulses after the capillary, the chirp of the pulses and the shape of the compressed pulses. This comparison clearly shows the linearizing effect of GVD when it acts together with SPM. It also shows a significant increase in quality of the compressed pulse. The time duration of the compressed pulse is slightly longer in the case where both effects are taken into account than in the case with only SPM. This is due to the fact that GVD broadens the pulse and thereby decreases the effect of SPM. All parameters but L_D are kept the same in the comparison.

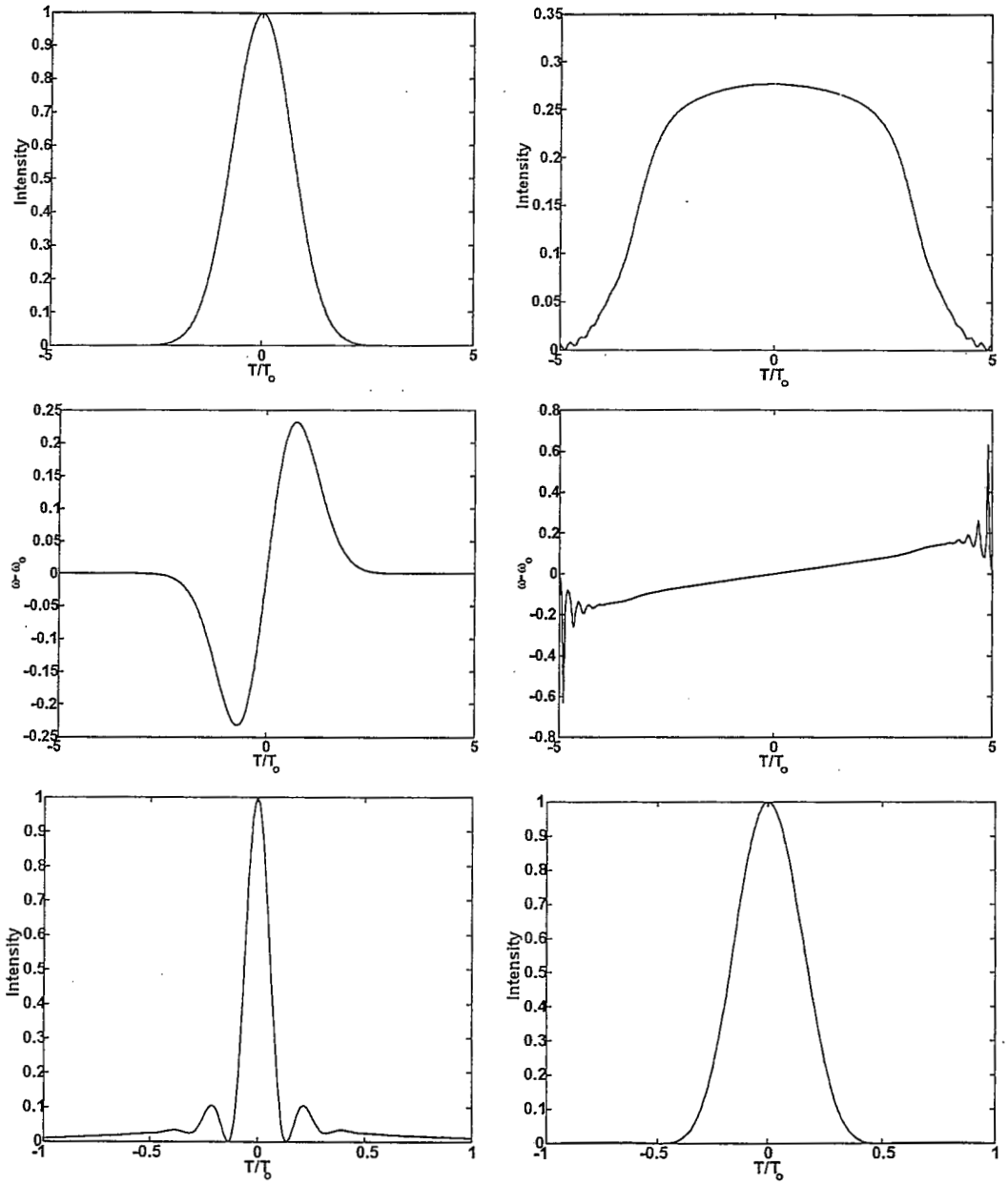

Figure 6. The pulse shape at capillary output, chirp and compressed pulse if GVD is excluded (left column) and included (right column). As the figure shows the quality of the compressed pulses can be significantly improved if GVD is included. The parameters used in the simulation are: $L = 2$ m, $L_{NL} = 0.1$ m. $L_D = \infty$ in the left column and 5 m in the right column. Note the different scale on the time axis used for the un-compressed and compressed pulses.

2.2.4 Higher order effects

If GVD and SPM where the only two effects it would be quite easy to produce very short pulses. However, the reality is not that simple. When the pulses become shorter higher order dispersion becomes increasingly significant. If the next term in the Taylor expansion (13) is added it is also possible to take the third order dispersion, TOD, into account. This is the term $i\frac{sgn(\beta_3)}{6L_D'}\frac{\partial^3 U}{\partial \tau^3}$ in equation (5) where $\beta_3 = \frac{\partial^3 \beta}{\partial \tau^3}$ and $L_D' = \frac{T_o^3}{|\beta_3|}$. This effect is only necessary to add if the pulses are very short (so that L_D' and L_D are comparable in magnitude) or if the GVD, for some reason, is close to zero. The TOD does not broaden the pulses symmetrically as the GVD, and it will make the trailing edge of the pulses longer and modulated. This modulation will rapidly decrease if the GVD is increased. The pulse shape of a pulse affected only by TOD is presented in Figure 7.

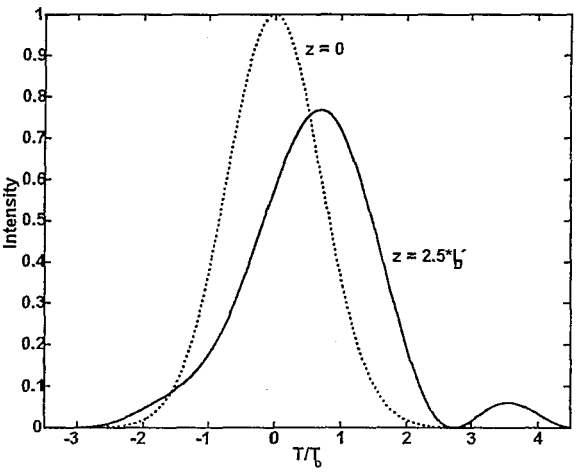

Figure 7. Pulse shape at $z = 2.5L_D'$ for a pulses affected only by TOD.

Another higher order effect comes from the fact that the refractive index does not change instantaneously as the intensity changes. Depending on the media it has a certain response time, T_R. The change in refractive index is due to a change in polarization of the media. This polarization can be achieved in different ways: electronic polarization which has a very fast response time, $T_R \simeq 5$ fs, or molecular orientation (not present in noble gases) which depending on the molecules has a response time ranging from $T_R \simeq 50$ fs to more than 1 ps [12]. If the response time is much shorter than the pulse duration it does not have to be included in the equation but can be regarded as instantaneous. If, on the other hand, the response time is much longer than the pulse it can also be neglected, since in this case it will not effect the pulses at all [14, 12]. Only if the response time and the pulse duration are comparable does this term need to be included. It will then lead to a red shift of the spectrum, which will also be more deeply modulated.

Another effect that has to be taken into account when the pulses are sufficiently short is the so-called self-steepening. This is introduced by the term

$$\frac{is}{L_{NL}}\frac{\partial}{\partial\tau}\left(|U|^2U\right), \tag{28}$$

in equation (5). Here s is the self-steepening parameter given by

$$s=\frac{2}{\omega_o T_o}. \tag{29}$$

This term acts as a intensity dependent GVD. That is, in normal material the parts of the pulse with high intensity will travel slower than the other parts, resulting in a reshaping of the pulse, thus making the trailing edge steeper. This is depicted in Figure 8.

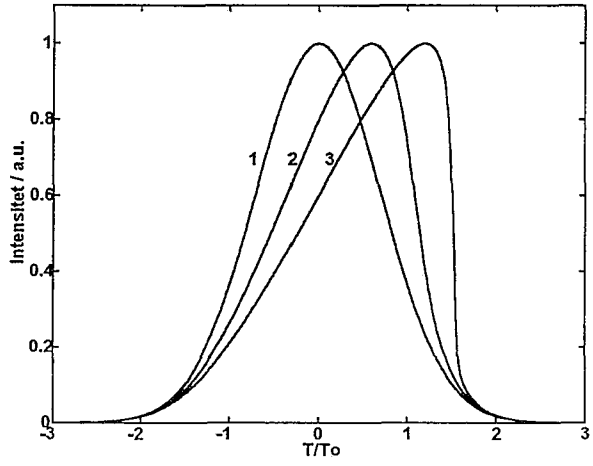

Figure 8. The figure shows how the pulse shape changes due to self-steepening. Curve number 1 is the unaffected pulse shape and number 2 and 3 are the pulse shapes after propagation different distances effected only by self-steepening.

This reshaping of the pulse will effect the SPM making the resulting spectrum asymmetric with greater broadening towards the blue, as depicted in Figure 9.

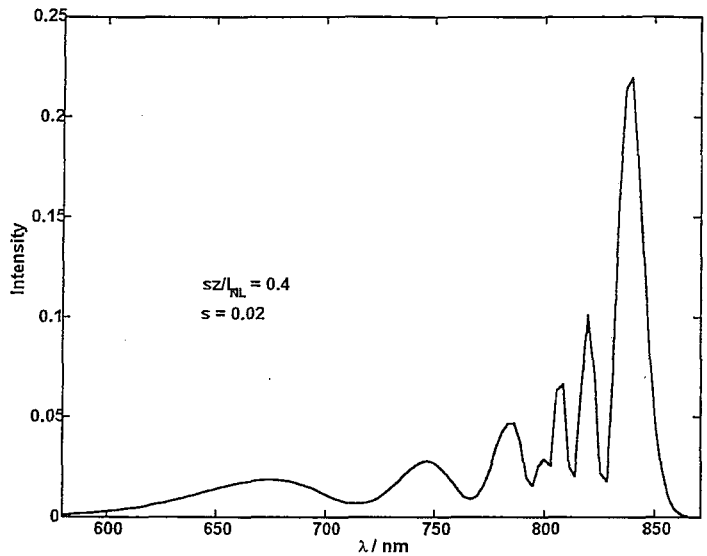

Figure 9. The spectrum at $\frac{sz}{L_{NL}} = 0.4$, where $s = 0.02$ and L_{LN} is the nonlinear length. The asymmetry in the spectrum is due to self-steepening. The effects of dispersion are neglected.

Exactly which effects that need to be taken into account depends on the time duration of the pulses and the geometry of the capillary.

2.3 Capillaries

The effects of GVD and SPM can be combined if the light, for example, is coupled into an optical fiber. This was done already in 1984 by Tomlinson *et al.*, [5]. The drawback with this method is that the energy must be very small (in the range of a few nJ) so that the fiber is not destroyed. Capillaries have been used as waveguides for a long time, for example in CO_2 *lasers*. In 1996 Svelto *et al.* showed that it was possible to compress pulses using a gas-filled capillary acting as waveguide, instead of the fiber [6,] (the spectral broadening was achieved in the capillary and the compression of the pulses where than obtained in a prism compressor). This method makes it possible to increase the energy since the gas will not be destroyed. Pulses with a duration shorter than 5 fs and with an energy of 0.5 mJ have since been produced [7]. It is possible to get a capillary to act as a waveguide, but since the refractive index of the gas inside the capillary is smaller than that of the surrounding walls it will not guide the waves as well as a fiber where the ratio is the inverse. In a fiber there might be total internal reflection for a large angle, while in a capillary all light must reflect at small angles (grazing incidence) if the losses are not to be too large. This makes it important to keep the capillary very straight. The waveguide properties in capillaries were studied in 1964 [8]. E. A. J. Marcatili and R. A. Schmeltzer found that the losses increase rapidly when the capillary is bent. The losses are approximately doubled if the radius of curvature is

10 km, which emphasizes the importance of keeping the capillary straight and suggests that it may be inconvenient to work with capillaries longer than ~ 1 m. When light is coupled into a capillary, three different transmission modes can be supported: transverse circular electric modes, transverse circular magnetic modes and hybrid modes where all electric and magnetic components are present. These modes are labeled TE_{0m} , TM_{0m} and EH_{nm} respectively. The indices n and m arise from the fact that all descriptions contains u_{nm}, which is a solution to

$$J_{n-1}(u_{nm}) = 0, \tag{30}$$

where J_{n-1} is the $n-1$ order Bessel function. If the refractive index of the external medium is more then 2.02 times the refractive index of the internal medium, then the mode with lowest attenuation is the TE_{01}. Otherwise EH_{11} will have the lowest attenuation [8]. In the case of a gas-filled fused silica capillary, the hybrid mode EH_{11} has the lowest losses and this mode will be studied in the following paragraphs.

The field in a EH_{11} mode is given by $J_o\left(2.405\frac{r}{a}\right)$ were J_o is the zero order Bessel function, a is the radius of the capillary and r is the radial coordinate.

The coupling efficiency $\eta = \frac{P_{out}}{P_{in}}$, where P_{in} and P_{out} are the input and output power respectively, is, for the EH_{1m}-modes, given by:

$$\eta = \frac{4\left[\int r J_o\left(u_{1m} r/a\right) \exp\left(-r^2/\omega^2\right) dr\right]^2}{\left[\omega^2 \int r J_o^2\left(u_{1m} r/a\right) dr\right]}, \tag{31}$$

[15, 16].

Figure 10 shows the calculated coupling efficiency, η, of the EH_{1m} modes ($m = 1, 2, 3, 4$) as a function of the input beam spot size, normalized to the capillary radius (ω/a). To couple as much energy as possible to the EH_{11} mode $\omega/a = 0.644$ turns out to be the optimum value. By proper mode-matching as much as ~ 98 % of the energy can, theoretically, be coupled to the EH_{11} mode. It is also noticeable that to have a coupling efficiency larger than 90 %, ω/a can range from 0.49 to 0.84.

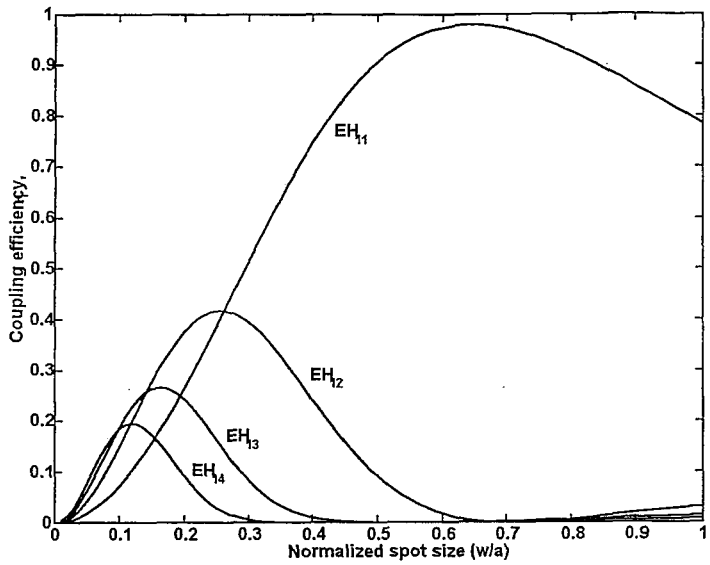

Figure 10. The coupling efficiency η for the hybrid modes EH_{1m} $(m = 1, 2, 3, 4)$ as a function of the normalized input spot size ω/a, where ω is the beam radius and a is the radius of the capillary.

The wave number due to the capillary is given by

$$\beta_{nm} = \frac{2\pi}{\lambda}\left[1 - \frac{1}{2}\left(\frac{u_{nm}\lambda}{2\pi a}\right)^2\right], \tag{32}$$

and the losses for the EH_{nm} modes are given by

$$\alpha_{nm} = \left(\frac{u_{nm}}{2\pi}\right)^2 \frac{\lambda^2}{2a^3}\frac{(\nu^2+1)}{\sqrt{\nu^2-1}}, \tag{33}$$

where ν is the ratio between the refractive indices of the capillary and the gas and α is the field attenuation constant. Equation (33) holds for a straight capillary and states that the losses increase if the radius a decreases and if the mode number nm increases, as depicted in Figure 11.

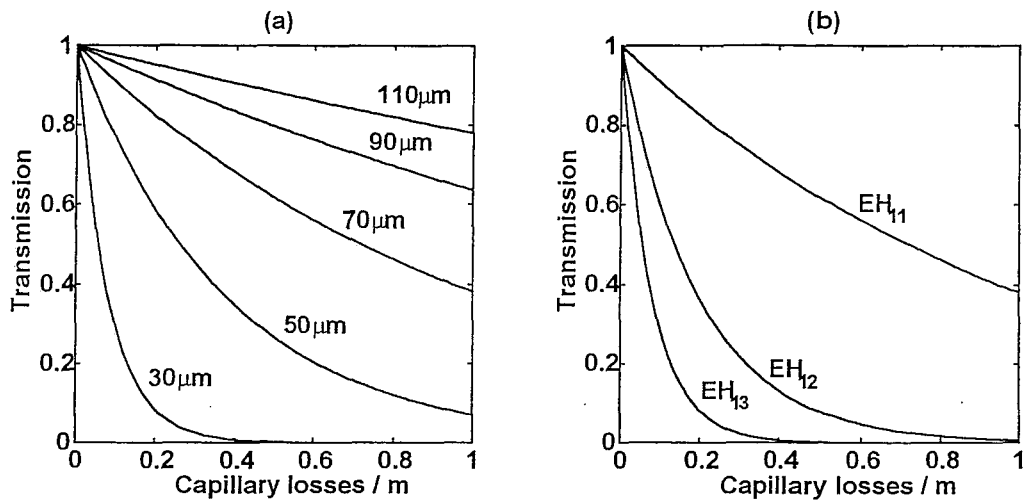

Figure 11. a) Transmission of the fundamental mode EH_{11} at 800 nm as a function of capillary length for different values of the capillary radius. b) Transmission of different modes (EH_{1m} $m = 1, 2, 3$) for a capillary radius of 70 μm as a function of capillary length.

In the remainder of this thesis, β_{11} will be referred to as β in order to simplify the notation. When the dispersion is to be studied equation (32) has to be used to evaluate $\beta_2 = \frac{\partial^2 \beta}{\partial \omega^2}$ and $\beta_3 = \frac{\partial^3 \beta}{\partial \omega^3}$ to get a correct value. According to [12] the effective area used to calculate the nonlinear coefficient γ in a capillary is given by:

$$A_{eff} = \frac{\left[\int\int_{-\infty}^{\infty} |F(x,y)|^2 \, dxdy\right]^2}{\int\int_{-\infty}^{\infty} |F(x,y)|^4 \, dxdy}, \tag{34}$$

where $F(x,y)$ is the modal distribution. If the fundamental mode, EH_{11}, is approximated by a Gaussian,

$$F(x,y) \simeq \exp\left(-\frac{x^2+y^2}{\omega^2}\right), \tag{35}$$

then equation (34) gives $A_{eff} = \pi\omega^2$. This is a factor 2 larger than the effective area used for Gaussian beams.

2.4 The compressor

To compress pulses with a chirp they have to pass through a device that introduces a chirp of opposite sign. Since the chirp of the pulse after the capillary is positive the chirp introduced by the compressor must be negative. There is no material with a dispersion such as to give the pulses a negative chirp (at least not in the wavelength region studied in this thesis, $\sim$ 800 nm). Due to this the compressor has to be designed in a more

complex way. There are several different alternatives for how the compressor could be designed. If the chirp is very large and linear and the pulses contain a lot of energy an arrangement of four gratings can be utilized to construct a good compressor.

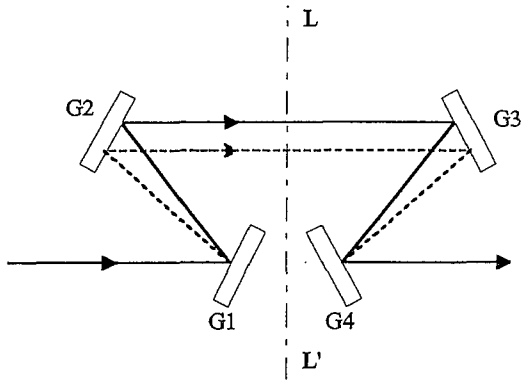

Figure 12. The grating compressor. G1-4 are gratings and LL' is a plane of symmetry. The solid line is a reference line and the incoming beam. The dashed line is the path a certain wavelength takes, different wavelengths makes different angles with the reference line and will thereby travel different path lengths. By introducing a mirror at the plane LL' only two gratings are needed to achieve the same grating sequence.

This compressor will be able to remove a positive linear chirp, arising from GVD, but it will not be able to compensate for higher order dispersion. The energy losses will be high even if blazed gratings[5] are used. The grating-compressor is a good alternative if the pulses contain a lot of energy and the chirp is close to linear. A grating compressor is used in many high-power laser systems [17].

Another alternative is to design dielectric mirrors so that they will introduce a certain amount of GVD and TOD every time the pulses are reflected [18]. Such mirrors are known as *chirped mirrors*. A compressor built of *chirped mirrors* will give the designer total control of the pulse properties. A drawback with a compressor built of only two chirped-mirrors is that you have to know exactly what the chirp looks like when the mirrors are being designed. Further more it is not possible to compensate in advance for dispersion introduced after the compressor. Normally the pulses are to be as short as possible in an experiment and on the way to it the pulses may pass different materials, air and glass for example, which introduces GVD. The compensation is achieved by introducing a small negative chirp on the pulses. If the setup is changed the amount of negative chirp introduced has to be changed and this is not possible if the compressor is built of two chirped mirrors. This type of compressor can only introduce small amount of dispersion and due to that they are not used to compress pulses after amplification.

A third alternative is to design the compressor with prisms, [9]. If the pulse passes four identical prisms it will be possible to introduce a negative chirp on the pulse.

[5] A blazed grating is a grating that is designed in such way that some energy is shifted out of the zeroth order into one of the higher order spectra.

Normally two prisms are used and the pulse passes each twice using a mirror. The prism compressor is the type used in the present thesis work.

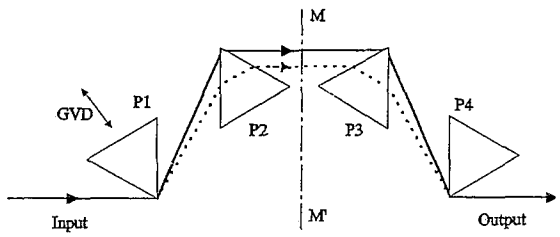

Figure 13. The prism compressor. P1-4 are identical prisms and the plane MM' is a plane of symmetry. Placing a mirror at MM' makes it possible to produce the same prism sequence using only two prisms. The arrow marked GVD shows how P1 can be translated to change the amount of material through which the pulses pass.

The idea behind the prism compressor is that different parts of the pulse (that is parts with different frequencies) should pass through different amounts of material. Since the first parts of the pulses have the lowest frequency the prism sequence has to be designed so that these frequencies pass through the largest amount of material. The first prism disperses the pulses spectrally, while the second and third introduce the chirp. The high-frequency parts of the pulse pass through the tip of the prism, so that they are almost not affected, while the low-frequency parts pass through more material and are slowed down relative to the high-frequency parts. The larger the distance between the prisms the greater the difference in the amount of material which the beam passes through and consequently the negative chirp introduced will be increased. The third and fourth prism also act as a collector and a collimator of the beam so that it will have the same size as before the compressor. If the compressor is well aligned there will be no difference in frequency across the pulses spatially. By moving the first prism back and fourth[6] the total amount of material the pulses pass through can be changed and in this way change the amount of GVD introduced. This makes it possible to compensate in advance for material that might appear after the compressor. In a prism compressor the beam size has to be small or different spatial parts of the pulse will be affected differently resulting in different time duration at different spatial locations. The small beam size reduces the maximum energy since the intensity in the prism cannot be too high because then there will be SPM in the material. The prism compressor is normally used in oscillators to compensate for the GVD introduced by the laser crystal, it is also the most common compressor for pulse compression using hollow waveguides. This compressor will, however, introduce some unwanted TOD. If the pulses are to be very short this compressor alone will not be sufficient.

If the pulses are to be very short, less than 10 fs, it is not enough to use only one of the above mentioned compressors, instead a combination of two of them has to be used to

[6]As indicated by the arrow marked GVD in Figure 13.

control the GVD and TOD independently. One combination is to use the prism compressor and the grating compressor. This was done in 1987 by Fork *et al.* together with a fiber to obtain a time duration of 6 fs, [2]. Another alternative is to use the prism compressor in combination with chirped-mirrors, [14]. The chirped mirrors are designed to introduce negative GVD and the prisms are then used to introduce GVD and TOD so that the total effect will be to remove all the GVD and TOD introduced by the capillary.

3 Experimental setup

3.1 Overview

The different parts of the experiment will be explained in detail in the forthcoming subsections of this chapter. This subsection presents the order of appearance of the parts. A few percent of the energy from the pulses from the terawatt laser are split of using the reflection on a beam splitter. These pulses are sent to the experimental setup where the pulse compression and diagnostics of the pulses are being performed.

The experimental setup is described in Figure 14. Once the beam is coupled out by M7 it is sent to the autocorrelator to be measured or to some further experiment or application.

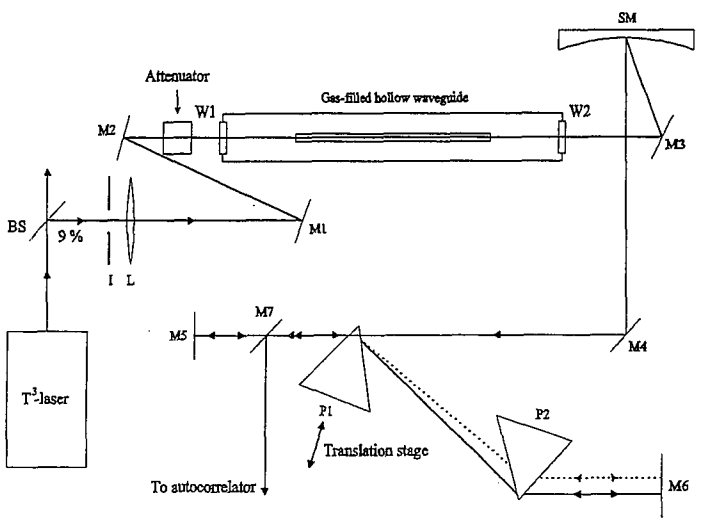

Figure 14. A drawing of the experiment. 9 % of the pulse energy from the T^3-laser is split of using a beam splitter, BS. The beam than passes an iris, I and is focused by the lens, L. Mirrors M1 and M2 are used to fold and steer the beam. The folding is needed due to the long focal length of the lens (2 m) compared to the space available on the table. The beam then passes a window, W1, and enters the capillary. M3 and M4 are mirrors used to steer and fold the beam. SM is a spherical mirror that collimates the diverging beam leaving the capillary. The compressor consists of mirrors M5, M6 and prisms P1, P2. After the compressor the beam is coupled out by the mirror M7.

3.2 The terawatt laser

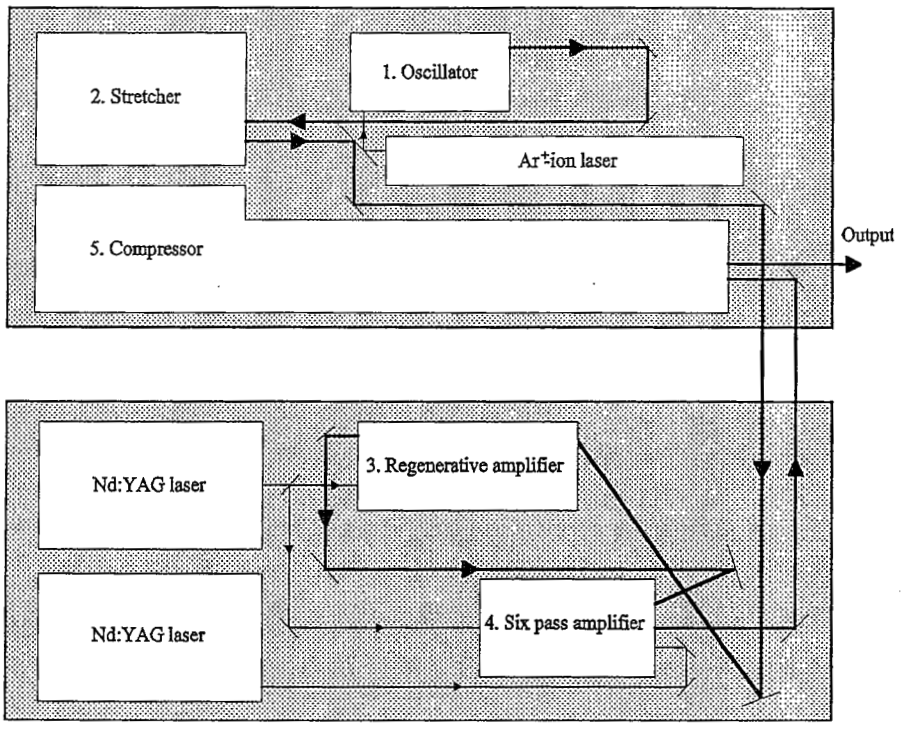

Figure 15. Schematic picture of the terawatt laser in Lund.

The laser used for the experiment is a Table Top Terawatt laser (T^3-laser). It generates 110 fs long pulses with 300 mJ per pulse at a repetition rate of 10 Hz corresponding to a maximum power of approximately 3 TW. The laser consists basically of 5 different components.

1. The oscillator. This produces short pulses with low energy ($\sim$ nJ) at a high repetition rate (76 MHz). An Ar^+-ion laser is used to pump the oscillator.
2. The stretcher. Using four passes on a grating the stretcher works as an inverted grating compressor, introducing positive dispersion. The time duration of the pulses increases 2500 times.
3. The regenerative amplifier. This selects pulses at 10 Hz and amplify these to approximately 5 mJ. It is pumped by a frequency doubled $Nd{:}YAG$ laser.
4. The six pass amplifier. This final amplifier increases the energy to maximum 600 mJ per pulse using six passes through a $Ti^{3+}{:}Al_2O_3$ crystal. This amplification stage is pumped by two frequency doubled $Nd{:}YAG$ lasers[7].

[7]Some of the energy from one of these lasers is used to pump the regenerative amplifier.

5. The compressor. The pulses are finally compressed to a time duration of $110fs$ in a grating compressor. Approximately half of the pulse energy is lost here[8] resulting in 300 mJ per pulse in the output pulses.

For a more detailed description of the system see [19] and for basic T^3–laser theory see [20, 17, 21, 22]. The grating compressor is to some extent explained in chapter 3.4.

If all the energy in the output pulses from the T^3–laser were to be coupled into the capillaries used in this thesis[9], the capillary would immediately be destroyed. For this reason, a beam splitter is used to split of 9 % of the energy. The back side of the beam splitter is anti-reflection coated to ensure that only reflections from the first surface are used. Since the reflections used comes from the first surface no dispersion will be introduced by the beam splitter.

For the capillary not to be destroyed the pulse energy coupled into it must not be much greater than 1 mJ. For this reason a variable attenuator is placed before the entrance of the capillary. This introduce also the possibility of altering the pulse energy coupled into the capillary.

3.3 The gas-filled hollow waveguide

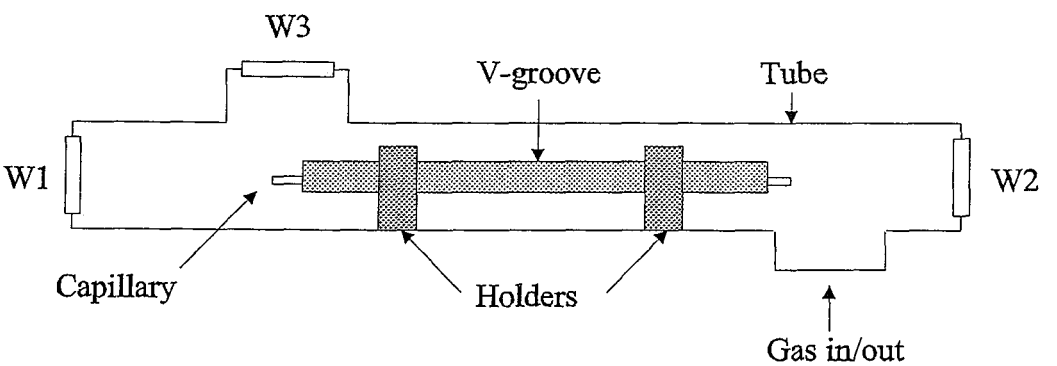

Figure 16. The capillary placed inside a gas cell in the shape of a tube. The beam enters through the window W1 and leaves through W2. The window W3 is placed so that it is possible to see the capillary entrance. The V-groove keeps the capillary straight and the holders centers the capillary in the tube.

As depicted in Figure 16 the capillary is placed in a V-groove so that it is kept perfectly straight. The V-groove is placed inside a tube with variable gas pressure. The ends of the tube are movable in all directions so that it is possible to align the capillary with

[8]The losses are due to the fact that not all the energy is reflected in the used order of reflection.
[9]The radius of the capillaries used alter from 110 to 130 μm.

the beam. It is important that the capillary is perfectly aligned with the beam since the wave guide properties of the capillary is not very good[10]. Once the capillary is aligned and the beam is focused into the capillary entrance the possibility to move the tube makes it possible to fine tune the position of the capillary so that the focus is perfectly centered. It is important that the focus is in the center of the capillary to couple to the EH_{11} mode.

The coupling of the beam into the capillary is brought about in the following way. When entering the system the pulses first passes trough an iris to be able to control the size of the beam. The size of the iris affects the size of the focal point. A smaller iris gives a larger beam waist in the focal plane, as discussed in appendix C. According to the theoretical discussion in Chapter 2.3 the size of the focal point is important to couple as much energy as possible to the lowest loss mode, the EH_{11} mode. To focus the beam a plano-convex spherical lens is used. The dispersion introduced to the pulses by the material in the lens is almost negligible. This is due to the fact that the time duration of the input pulses is quite long (110 fs). The dispersion length, L_D, of fused silica will then be approximately 0.12 m and a 110 fs pulse will be 110.01 fs long after having passed 2 mm of fused silica (according to equation (16)). If the pulses had been shorter, a spherical mirror had been a better focusing element since the dispersion increases with decreasing time duration. In the next step the pulses pass two mirrors used to guide the beam and an attenuator used to change the energy of the pulses. The pulses then passes a 1.5 mm thick glass window (if the input pulses are shorter, the thickness must be decreased to minimize dispersion) placed as far from the capillary entrance as possible so that the beam size is still quite large and the effect of SPM in the material is minimized. The capillary entrance is placed in the focal point and the pulses are guided through the capillary. They leave the tube through a 1.5 mm thick glass window and are then collimated by a spherical gold mirror with a focal length of 0.5 m. The focal length is chosen such that the size of the beam is quite small, but not too small, $\omega \simeq 1$ mm[11].

3.4 The prism compressor

The compressor is built of two fused silica prisms with an apex angle of 69°. The angle is chosen such that the beam will enter the prisms at Brewster angle when the prisms are aligned for minimum deviation and thereby minimize the reflection losses[12]. The compressor is designed as depicted in Figure 13 with a mirror inserted at the plane of symmetry, MM'.

[10] See chapter 2.3

[11] If the beam size is too large the prism compressor will affect different parts of the pulse differently. If the beam size is too small the pulses will be affected by SPM in the material in the compressor.

[12] The angle for minimum deviation is easy to find and ensures that the beam travels parallel to the base of the prism.

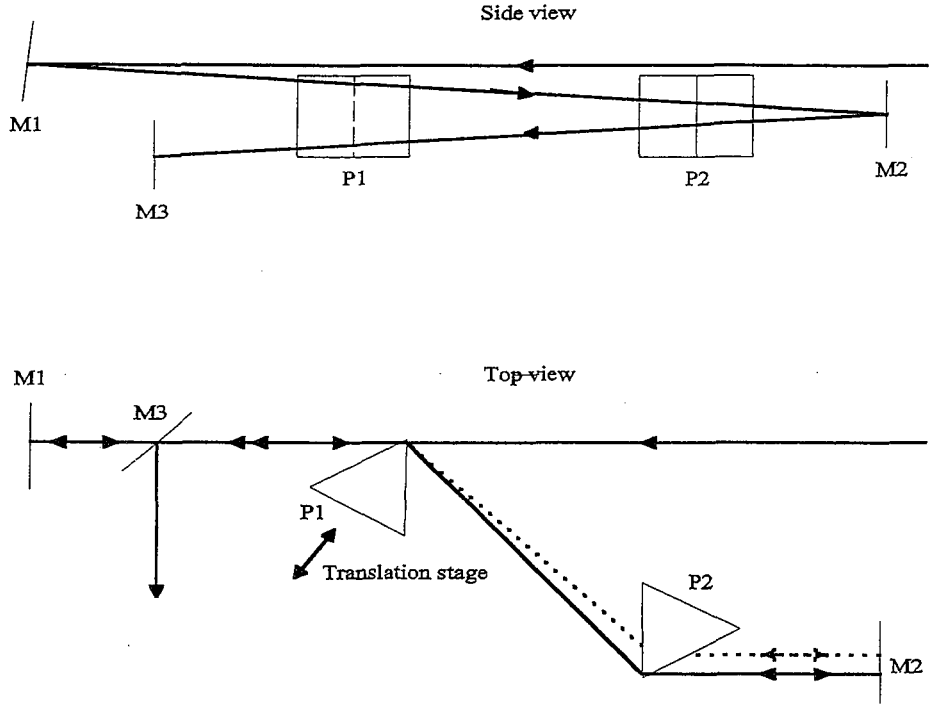

Figure 17. The prism compressor viewed from the side (upper picture) and from above (lower picture).

With labeling according to Figure 17: the beam first passes above the first prism (P1) and onto a mirror (M1), which is tilted slightly downwards, and then trough P1. The second prism (P2) is positioned so that the high frequency part of the beam passes just at the tip of P2 while the low frequency parts passes more material. The beam is then reflected by a vertical mirror (M2), this ensures that the beam passes the same amount of material on the way back. P1 is placed on a translation stage. This makes it possible to change the dispersion introduced by the compressor. If there is a need to introduce more negative dispersion than is possible only by moving P1, the distance between P1 and P2 has to be increased [9]. After the compressor the beam is coupled out using a third mirror (M3) and sent to the autocorrelator.

3.5 The autocorrelator

To measure the time duration of the compressed laser pulses a multi shot autocorrelator was built (for the theory regarding multi shot autocorrelators see appendix F.1). This technique uses several pulses to measure the time duration which makes it reliable only if all the pulses have the same appearance. However, it was found that the energy and appearance of the input pulses from the T^3 laser, fluctuated, on a shot–to–shot basis. The conditions where therefore not the same for all the pulses. This made the

measured output time duration fluctuating and difficult to trust. A commercial single shot autocorrelator was therefore used instead. This measures the time duration of the pulses using only one pulse for each measurement (for the theory regarding single shot autocorrelators see appendix F.2). This autocorrelator was, however, designed for longer pulses ($\tau \simeq 100$ fs) than the compressed pulses. The multishot autocorrelator was rebuilt as a single shoot with a resolution sufficient to measure the compressed pulses. Unfortunately, due to an extended service period on the T^3 laser system, the testing of this new autocorrelator could not be performed before the writing of the present thesis.

4 Results

This section is divided into several parts. The first part deals with the coupling of the beam into the capillary and the output mode structure. The second part presents measurements of the broadened spectra and the time duration after the compressor. The third part present the simulation program used to simulate the propagation of the laser pulses.

4.1 Coupling into the capillary

According to the theory, outlined in Chapter 3.3, the size of the beam radius, when entering the capillary, should be 65 % of the capillary radius (Figure 18 c) in order to couple as much energy as possible to the EH_{11} mode. To measure the coupling efficiency a variable aperture was used to change the beam size before the lens (and thereby the beam waist diameter in the focal plane). When the aperture size is changed the position of the focal plane will also be slightly altered, [20], and this has to be adjusted for. The energy was measured before and after the capillary and the ratios were plotted.

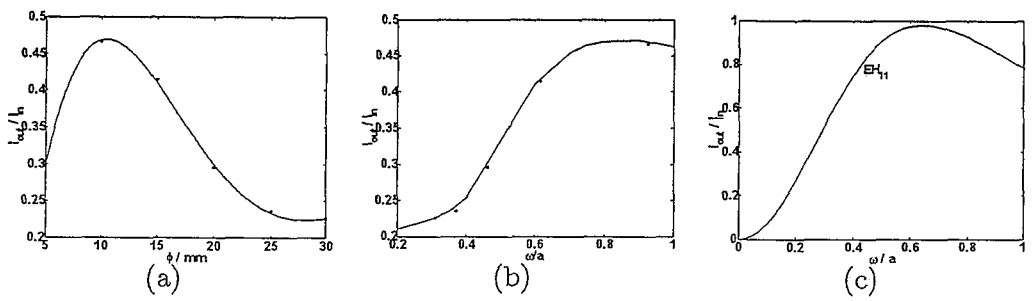

Figure 18. a) The ratios between measured input and output energy as a function of input beam diameter. The capillary was 65 cm long and the radius was 110 μm. b) Same as a), but the x-axis is changed to the ratio between the size of the focus and the radius of the capillary. c) Theoretical calculations of the coupling efficiency to the EH_{11} mode.

Figure 18 a and b show the results of the experimental coupling ratios. Figure 18 a shows the ratios as a function of the size of the iris. This result is convenient to use when the experiment is preformed and the throughput is optimized. To compare the experimental results with theory the x-axis is recalculated and displayed in Figure 18 b as the ratio between the size of the focus and the radius of the capillary[13]. Figure 18 c shows the theoretically calculated coupling efficiencies for the EH_{11} mode. To compare the experimental results with the theoretical, Figure 18 b and c are used. The curve corresponding to the coupling to the EH_{11} mode in Figure 18 c are used since

[13]The theory of focusing Gaussian beams is explained in appendix C.

most of the energy in the experiment is coupled into this mode[14]. The two curves have approximately the same appearance, but the maximum value of the experimental curve is much lower than the theoretical. The high losses in the experiment can mainly be attributed to three reasons:

1. The theoretical curve does not take into account the losses when passing the capillary.
2. The laser beam was slightly astigmatic.
3. The theoretical calculations assumes a Gaussian shape of the input beam. The spatial shape of the beam used in the experiment was not Gaussian. When such input mode is coupled into the capillary the capillary will act as a spatial filter, removing the parts of the pulse that are not coupled to the EH_{11} mode (since these have higher losses). This result in a nice spatial shape of the output pulse but the energy is reduced.

In the experiment, most energy was coupled into the capillary when the beam size was slightly larger than predicted by theory. This can be attributed to the fact that the pulse, after having passed the iris, is no longer well approximated by a Gaussian shape. The pulse shape at the focal point depends on the input pulse shape. If the input pulse shape is Gaussian, the beam profile at the focal plane will also be Gaussian, but if the input pulse shape is a square pulse, the pulse shape at the focal point will be given by:

$$I(\theta) = I(0)\left[\frac{2J_1(\gamma)}{\gamma}\right]^2, \tag{36}$$

$$\gamma = \frac{2\pi a}{\lambda}\sin\theta \tag{37}$$

known as an Airy pattern. J_1 is the first order Bessel function, a is the radius of the capillary and θ is the angle from the centre line [23].

[14]Some of the energy will be coupled into the other modes as well, but since these have such high losses when the pulses pass the capillary the output will mostly be due to the energy coupled into the EH_{11}mode. The coupling to the other modes will, however, increase the losses.

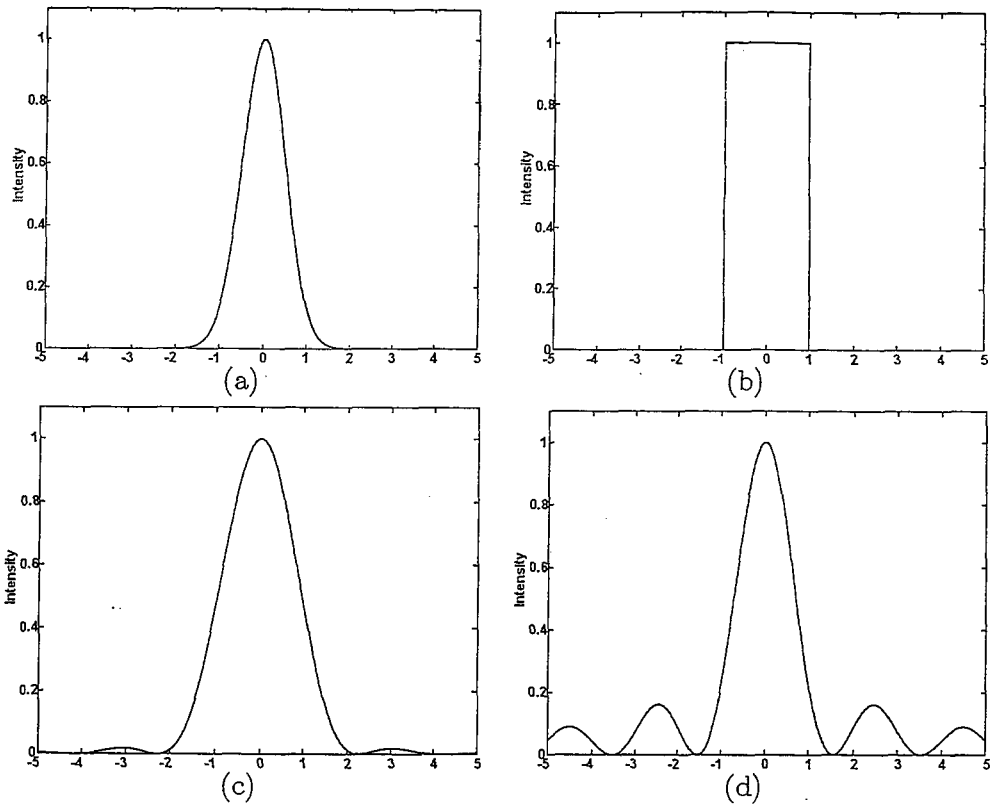

Figure 19. Different spatial pulse shapes. The x-axes are displayed with arbitrary units since the curves are presented merely too compare the shapes. The different graphs are: a) Gaussian pulse shape. b) Top-hat. c) The intensity distribution across the Airy pattern d) Bessel function squared, this is the shape of the EH_{11} mode which the input beam is to be coupled to.

When the iris is fully opened the input pulse shape much resembles a Gaussian pulse shape, but when it is almost closed a top-hat will be a better approximation. In-between these positions it will be a truncated Gaussian resulting in a shape at the focal point somewhere between a Gaussian pulse shape and an Airy pattern.

When a capillary with larger radius (130 μm) was used the result was approximately the same, but the maximum occurred at a smaller input beam size (as it should to have the same ratio ω/a).

The appearance of the output mode is strongly dependent on the size of the focal point, that the beam is centered at the capillary entrance and that the capillary is parallel to the optical axis of the laser beam. If the size of the focal point is too small the amount of energy coupled to other modes than EH_{11} will increase. This will increase the losses and the output mode will be a combination of several different modes. If the size of the focal point is too big approximately the same will happen, but in this case a lot of

energy will be lost at the entrance of the capillary, possibly causing optical damage.

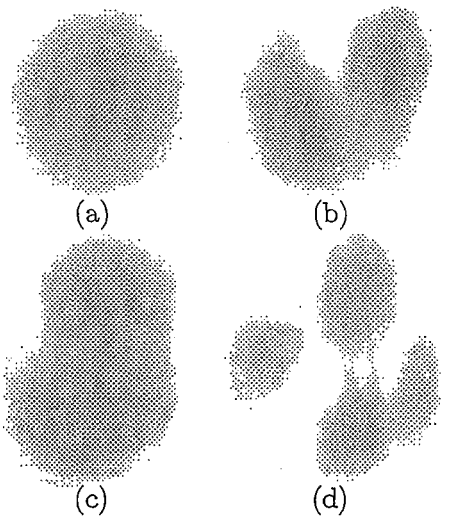

Figure 20. The output pulse shape when a) everything is optimized. b) the iris is opened slightly more than optimum. c) the input entrance is located slightly of the focal point. d) the iris is opened even more compared to b).

The pictures in Figure 20 are taken using a CCD-camera placed after the capillary. When the coupling was not optimized to the EH_{11} mode the shape of the output pulses fluctuated quite a lot. The pictures are therefore not the only occurring shapes for the different conditions, but they are typical. To couple the beam to the EH_{11} mode only was difficult since the focus was slightly astigmatic due to the laser, resulting in two focal points spaced approximately 3 cm. In addition, the input mode was not a pure Gaussian but quite irregular. This made it inevitable that some of the energy was lost at the entrance and some energy coupled to other modes than the EH_{11}. When the coupling to EH_{11} was optimized the output mode consisted almost only of that mode. This is due to the high losses in the capillary for the other modes. The output energy was, however, only half of the theoretical value[15], but this can be explained by the losses at the entrance and the coupling to high loss modes (EH_{12}, EH_{13} etc.).

[15]The theoretical value is 98 % of the input energy. This is the maximum in figure 18 c.

4.2 Broadened spectra and compressed pulses

To characterize the compressed pulses the spectrum and the time duration were measured. Two different spectrometers were used to measure the spectrum. The first was an ordinary spectrometer consisting of an input slit, two mirrors, a grating and a CCD-array. The resulting spectra all showed an anomalous feature with peaks which were not affected by the capillary.

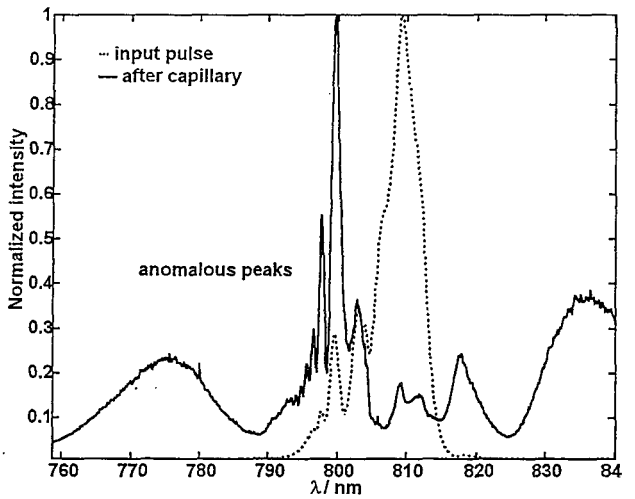

Figure 21. A spectrum with the anomalous peaks. To record the spectra the fiber-coupled grating spectrometer was used. The broadened spectrum is truncated due to the choice of grating (a high resolution was needed to resolve the peaks). The radius of the capillary was 110 μm and the pressure was increased until the anomalous peaks were clearly visible (more than 3 bars).

The anomalous peaks are displayed in the central part of Figure 21 (around 800 nm). The input pulse contain the same feature as the output and the anomalous peaks are located at the same wavelengths. It was assumed that something was wrong with the spectrometer and another one was used to test this hypothesis. The second spectrometer used was a fiber-coupled grating spectrometer. This spectrometer uses a fiber to collect the light to be measured and has four different gratings (with different number of lines per length unit) so that the resolution can be changed. To avoid nonlinear effects in the fiber (such as SPM) the intensity has to be very low and therefore the diffuse reflection from a tarnished surface was used. With this spectrometer the spectra still showed the same anomalous feature as with the first spectrometer and the conclusion was that this was the actual appearance of the spectra.

The anomalous parts of the spectrum was not affected by the capillary (the appearance did, for example, not change when the pressure was changed). This observation lead to the assumption that the anomalous peaks in the spectra arises due to a long pedestal in the input pulses. If the pedestal is sufficiently long, and the power therefore low, SPM

will not affect its spectrum. The laser system was investigated and it was found that the strange spectrum was arising in the regenerative amplifier. A long pedestal will not affect the compressibility of the pulses since it does not affect the main parts of the pulses. The evaluation of the measured spectra will, however, be more difficult. The pedestal will also make it more difficult to simulate the conditions at hand since it is hard to know how much of the energy that is contained in the main pulse.

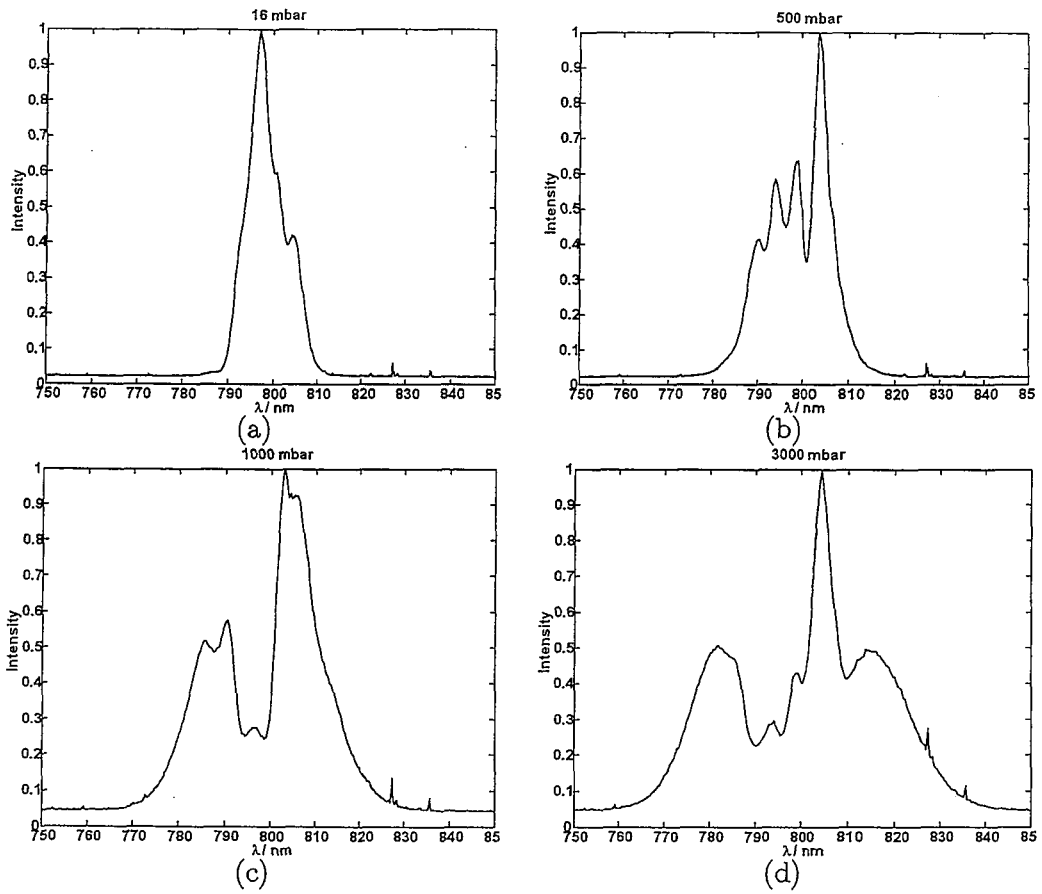

Figure 22. The spectral broadening when the pressure is increased. The radius of the capillary used was 110 μm and the energy is 0.75 mJ per pulse. The pressure in the different pictures are: a) 16 mbar b) 500 mbar c) 1000 mbar and d) 3000 mbar.

Aside from the anomalous peaks in the spectrum the spectral broadening due to the capillary was in accordance with the theory in chapter 2.2.2 and 2.2.3. For example, the spectrum was broadened when the pressure was increased, as illustrated in Figure 22. The gas used in most experiments was argon with

$$\frac{n_2}{p} = 9.8 \cdot 10^{-24}\ m^2/Wbar, \tag{38}$$

where n_2 is the nonlinear refractive index and p is the pressure [3]. According to [24] (38) is valid for pressures greater than a few 100 $mbar$, but at lower pressures the value

of n_2 is approximately constant. There is a large uncertainty in the value of n_2 due to the difficulty of measuring it.

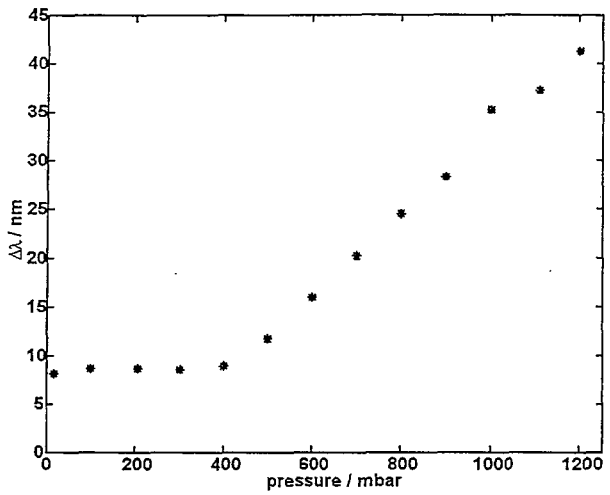

Figure 23. The broadening of the spectrum as a function of pressure. The input energy was 0.75 mJ per pulse, the radius of the capillary was 110 μm and the gas used was argon. The anomalous peaks was removed in the measurements of the full-width-at-half-maximum of the spectra.

According to Figure 23 the FWHM of the spectrum does not start to increase until the pressure has reached about 400 mbar. This is at a somewhat higher value than predicted in [24].

When the pressure is increased even further, the spectral width starts to increase more slowly and might reach a maximum when the pressure is well above 3 bars. However, the gas handling system used was not designed for high pressures, which limited the investigated pressure range to $0 - 3$ bars.

After the pulses had passed the capillary they were collimated using a spherical mirror with a focal length of 0.5 m. The reason for using a spherical mirror instead of a lens was to avoid unnecessary dispersion due to material[16]. To reduce the astigmatism introduced by the mirror, the angle between the incident and reflected beam was made as small as possible. The beam was than sent to the prism compressor.

The prisms in the compressor was adjusted so that the sides were perfectly vertical. The spacing between the prisms, $\sim$ 65 cm, was chosen such that zero GVD was introduced when the beam passed approximately at the center of the first prism, [9, 11]. After the compression the pulses were sent to the autocorrelator to be measured. All presented data are recorded using the commercial single shot autocorrelator.

[16]The effect of dispersion in material is increased when the spectrum of the pulse is broadened.

The signal from the autocorrelator was displayed using an oscilloscope. Once a trace was recorded the data was transferred to a computer and a Gaussian trace was fitted to the autocorrelation trace. In Figure 24 one of the first recorded autocorrelation traces of a compressed pulse is displayed.

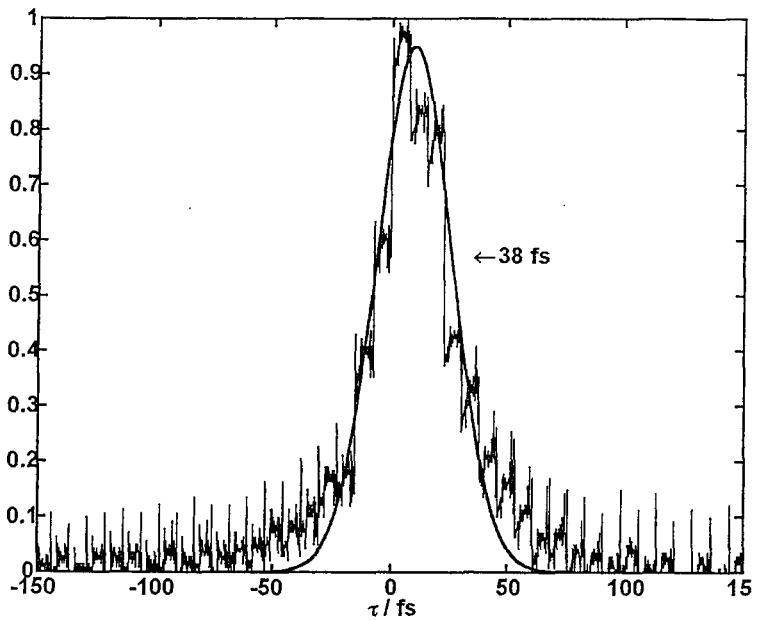

Figure 24. One of the first autocorrelation traces of a compressed laser pulse. The time scale is calculated assuming a $sech^2$ shape of the pulse and the full width half maximum is 38 fs.

To optimize the compressor, several traces were recorded and evaluated for different positions of the first prism. The position is the reading on the micrometer screw that controls the translation stage for the first prism. A decrease in the value of the position corresponds to an increase in amount of material the pulses pass in the first prism. At the entrance of the autocorrelator there is a several mm thick filter. For the recorded pulses to be as short as possible the compressor had to be adjusted to compensate in advance for the dispersion introduced by this filter and the nonlinear crystal.

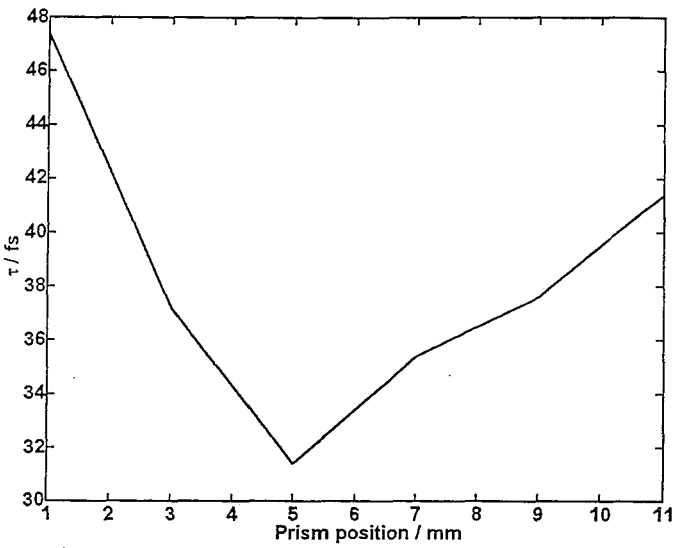

Figure 25. The average time duration for different prism position. The pressure of the argon gas in the capillary was 1.7 bars, the input energy was 0.65 mJ per pulse and the radius of the capillary was 110 μm.

In Figure 25 the time duration for a pressure of 1.7 bars argon and an input energy 0.65 mJ per pulse is displayed for different readings on the micrometer screw. The reason for the asymmetry in Figure 25 might be that more TOD is introduced when the amount of material is increased resulting in longer time duration. The shortest time duration displayed in Figure 25 is 31.4 fs. This is the average value of several traces and the best result at these condition was 29 fs. The fluctuations of the signal was approximately within ± 3 fs.

When the conditions were changed to an input energy of 1.3 mJ and a pressure of 1.2 bars the best result was a pulse duration of 25 fs. The energy after the capillary under these conditions was 0.45 mJ. The FWHM of the spectrum was 65 nm and should, if $sech^2$ shape is assumed, be able to support 10 fs pulses. This means that the achieved pulses were approximately 2.5 times transform limited. The reasons for the pulses not to be transform limited was because of the incapability to remove the TOD with the compressor and that the combination of SPM and GVD in the capillary was not optimal.

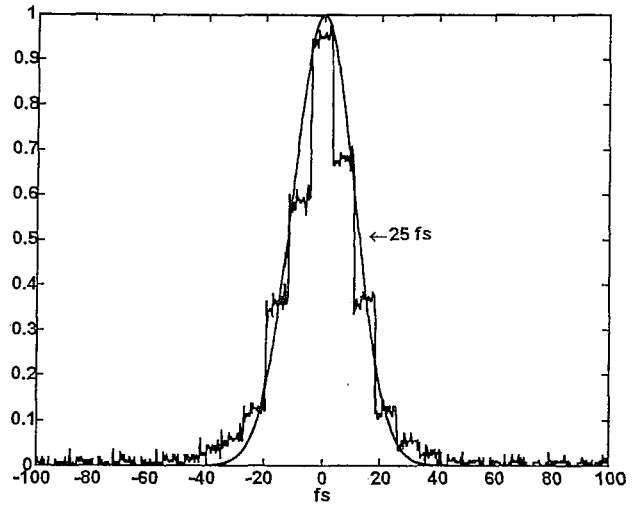

Figure 26. The autocorrelation trace of the 25 fs long pulse. The recorded data and a fitted Gaussian pulse shape. The input energy was 1.3 mJ per pulse and the pressure 1.2 bars of argon.

For the 65 cm long capillary with a radius of 110 μm several different conditions were investigated to see which gave the shortest pulses. Some of the data is presented in Table 1.

Gas	*pressure / mbar*	E_{in} / *mJ*	τ_{FWHM} / *fs*
air	1013	0.63	50
air	1013	0.83	50
Ar	1200	0.38	40
Ar	1200	0.65	29
Ar	1200	0.73	32
Ar	1200	1.3	25

Table 1. Results for different conditions. The capillary was 65 cm long and the radius was 110 μm.

The best result using this capillary was 25 fs long pulses achieved with 1200 mbar of argon and an input energy of 1.3 mJ per pulse, depicted in Figure 26. For all different combinations presented in Table 1 it was possible to compress the pulses to 50 fs or less. However, it was not always possible to get a nice shape on the output pulse. Using air with atmospheric pressure and an input energy of 0.83 mJ, for example, resulted in pulses with pre- and/or post-pulses. An autocorrelation trace of a pulse recorder under those conditions is presented in Figure 27.

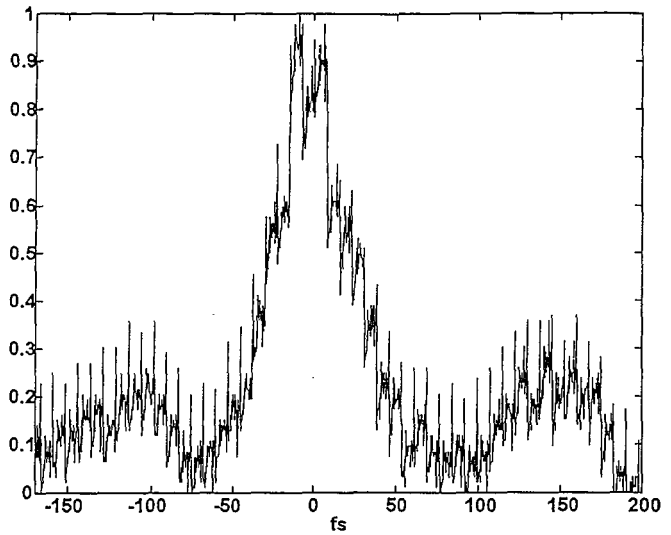

Figure 27. An autocorrelation trace with pre- and/or post-pulses. The gas is air at 1 atm and the input energy is 0.83 mJ per pulse.

If the radius of the capillary is increased the effect of GVD will increase compared to SPM. To examine if this would decrease the time duration of the compressed pulses the capillary was changed to another one with a 130 μm radius. The first experiment with the new capillary was performed using air at 1 atm. The spectra of the output pulses in Figure 28 a was less modulated than the spectra recorded after the capillary with a radius of 110 μm (the anomalous peaks has to be neglected). This is expected when the GVD is increased and is simulated in the next subsection. When the pulses where compressed the resulting time duration was as short as 13 fs as displayed in Figure 28 b. The energy of the compressed pulses, with 13 fs time duration, was 0.3 mJ resulting in a total power of $\frac{0.3 \text{ mJ}}{13 \text{ fs}} = 23$ GW.

The resolution was limited by the pixel size in the CCD-array[17]. Therefore the pulse depicted in Figure 28 b might have a time duration shorter than 13 fs. The pulse may also have pre- and/or post-pulses that are not resolved in the figure.

[17]Each step in the trace represents a pixel on the CCD-array.

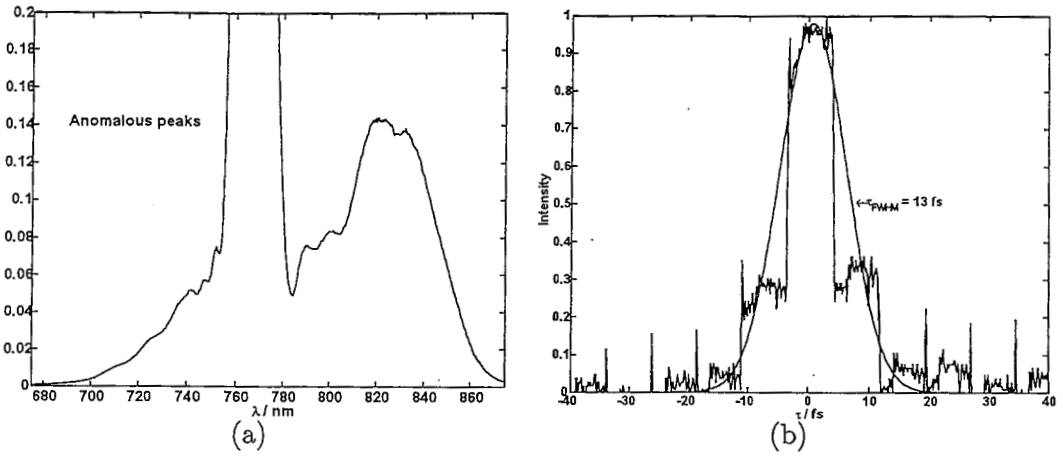

Figure 28. a) The spectrum of the shortest pulse produced. b) The autocorrelation trace of the shortest pulse produced, 13 fs. The gas used was air at 1 atm and the radius of the capillary was 130 μm.

4.3 Simulations

A Matlab based program was developed to simulate the propagation of the pulses. The method used is the symmetrized split-step Fourier method, described in appendix B, with three iterations when the non-linear part is calculated. In the program it is possible to include the effects of: GVD, TOD, SPM, Self-steepening and non-instantaneous response time. To make sure that the program works correctly comparisons are made with results that are possible to calculate analytically and results published in [12]. All calculated pulse shapes and spectra presented in this thesis that were not possible to calculate analytically are simulated using this program. A further description of the program will later be presented in a separate report.

5 Summary and outlook

In this master thesis a new pulse compression technique using a gas-filled hollow waveguide has been implemented for the 110 fs, 10 Hz terawatt laser in Lund. This technique uses the combined effects of self phase modulation and group velocity dispersion to broaden the spectrum of the pulses and to produce a linear chirp. This chirp is then removed, and the pulses compressed in time, using a prism compressor.

A significant decrease in time duration was achieved. The shortest measured pulses had a time duration of 13 fs. The energy of these pulses was 0.3 mJ.

To improve the system a spatial filter can be used in the laser beam to avoid the problems of astigmatism and irregular beam profile. This will make it possible to couple more energy into the capillary without optical damage. The diagnostics should be improved by using the single shot autocorrelator designed for very short pulses. Even better would be to measure simultaneously the chirp of the pulses and the time duration, [25, 26]. One of the challenges using this technique with 110 fs is that the effect of GVD will be too small relative to the effect of SPM. The technique is better suited for compressing pulses that are already short to start with, since this will increase the effect of GVD. At the Lund High-Power Laser Facility there is a laser producing pulses with a time duration of 30 fs at a repetition rate of 1 kHz. The next step will be to implement the technique on that system and compress those pulses to less than 10 fs. The compressed pulses will than be used to measure the time duration of the high order harmonics produced using the same laser. Eventually the pulses will also be used to produce ultrashort pulse harmonics.

6 Acknowledgements

First of all I would like to thank my supervisor Claes-Göran Wahlström for his guidance and support during this thesis work. Through his questions he challenged me to improve upon my approaches to this experiment.

I would also like to thank:

- Oliver Dühr for many interesting discussions about the pulse compression technique in specific, and about lasers and atomic physics in general. He also helped in correcting some theoretical mistakes in this thesis.
- Jim Smith for making the text more readable by correcting the grammar and for helping me to find the appropriate words.
- The Ph.D. students Anders Sjögren and Christian Delfin, who have patiently answered many questions and helped me to find different parts for my experimental setup.
- Anders Persson, who has helped me with the laser.
- The Lundberg family, for lending me their computers to run the simulation program.
- All not mentioned here, but not forgotten.

Finally I would like to thank my girlfriend Jessica for putting up with me even when autocorrelation traces started to appear in our apartment, and for helping me to structure this thesis.

References

[1] S. De Silvestri, P. Laporta, and V. Magni. Generation and applications of femtosecond laser pulses. *Europhys. news*, 17(9):105–108, 1986.

[2] R. L. Fork, C. H. Brito, P. C. Becker, and C. V. Shank. Compression of optical pulses to six femtoseconds by using cubic phase compensation. *Opt. Lett.*, 12(7):483–485, 1987.

[3] M. Nisoli, S. De Silvestri, O. Svelto, R. Szipöcs, K. Ferencz, Ch. Spielmann, S. Sartania, and F. Krausz. Compression of high-energy laserpulses below 5-fs. *Opt. Lett.*, 22(8):522–524, 1997.

[4] P. M. W. French. The generation of ultrashort laser pulses. *Rep. Prog. Phys.*, 58:169–267, 1995.

[5] W. J. Tomlinson, R. H. Stolen, and C. V. Shank. Compression of optical pulses chirped by self-phase modulation in fibers. *J. Opt. Soc. Am. B*, 1(2):139–149, 1984.

[6] M. Nisoli, S. De Silvestri, and O. Svelto. Generation of high energy 10 fs pulses by a new pulse compression technique. *Appl. Phys. Lett.*, 68(20):2793–2795, 1996.

[7] S. Sartania, Z. Cheng, M. Lenzner, G. Tempea, Ch. Spielmann, F. Krausz, and K. Ferencz. Generation of 0.1-tw 5-fs optical pulses at a 1-khz repetion rate. *Opt. Lett.*, 22(20):1562–1564, 1997.

[8] E.A.J Marcatili and R. A. Schmeltzer. Hollow metallic dieletric waveguides for long distance optical transmission and lasers. *Bell Syst. Tech. J.*, pages 1783–1809, 1964.

[9] R. L. Fork, O. E. Martinez, and J. P. Gordon. Negative dispersion using pairs of prisms. *Opt. Lett.*, 9(5):150–153, 1984.

[10] J. M. Schins, P. Breger, P. Agostini, R. C. Constantinescu, H. G. Muller A. Bouhal, G. Grillon, A. Antonetti, and A. Mysyrowicz. Cross-correlation measurements of femtosecond extreme-ultraviolet high-order harmonics. *J. Opt. Soc. Am. B*, 13(1):197–200, 1996.

[11] J.-C. Diels and W. Rudolph. *Ultrashort laser pulse phenomena.* Academic Press, 1996.

[12] G. P. Agrawal. *Nonlinear fiber optics.* Academic Press, 1989.

[13] O. Svelto. *Principles of lasers.* Plenum, 1998.

[14] M. Nisoli, S. Stagira, S. De Silvestri, O. Svelto, Ch. Spielmann M. Lenzner, S. Sartania, and F. Krausz. A novel - high energy pulse compression system: Generation of multigigawatt sub-5-fs pulses. *Appl. Phys. B*, 65:189–196, 1997.

[15] M. Nisoli, S. Stagira, S. De Silvestri, O. Svelto, S. Sartania, Z. Cheng, G. Tempea, C. Spielmann, and F. Krausz. Toward a terawatt-scale sub-10-fs laser technology. *IEEE J. selected topics in Quantum Electron.*, 4(2):414–419, 1998.

[16] W. Heuer and H. Zacharias. Stimulated raman effect and four-wave mixing in a hollow waveguide. *IEEE J. Quantum Electron.*, 24(10):2087–2100, 1988.

[17] M. H. R. Hutchinson. Terawatt lasers. *Contemp. Phys.*, 30(5):355–365, 1989.

[18] R. Szipöcs, K. Ferencz, C. Spielmann, and F. Krausz. Chirped multilayer coatings for broadband dispersion control in femtosecond lasers. *Opt. Lett.*, 19(3):201–203, 1994.

[19] S. Svanberg, J. Larsson, A. Persson, and C.-G. Wahlström. Lund high-power laser facility — systems and first results. *Physica Scripta*, 49:187–197, 1994.

[20] A. E. Siegman. *Lasers.* University Science Books, 1986.

[21] P. M. W. French. Ultrafast solid-state lasers. *Contemp. Phys.*, 37(4):283–301, 1996.

[22] S. Backus, C. G. Durfee III, M. M. Murnane, and H. C. Kapteyn. High power ultrafast lasers. *Rev. Sci. Instrum.*, 69(3):1207–1223, 1998.

[23] E. Hecht. *Optics.* Addison-Wesley Publishing Company, 1987.

[24] H. J. Lehmeier, W. Leupacher, and A. Penzkofer. Nonresonant third order hyperpolarizability of rare gases and n_2 determined by third harmonic generation. *Opt. Commun.*, 56(1):67–73, 1985.

[25] M. A. Franco, J.-F. Ripoche, H. R. Lange, J. P. Chambaret, P. Rousseau, B. S. Prade, and A. Mysyrowicz. How to measure femtosecond pulses. *American Institute of Physics, Conference Proceedings 426, Superstrong Fields in Plasmas: First International Conference, Edited by M. Lontano, G. Mourou, F. Pegoraro and E. Sindoni*, pages 423–437, 1997.

[26] B. S. Prade, J. M. Schins, E. T. J. Nibbering, M. A. Franco, and A. Mysyrowicz. A simple method for the determination of the intensity and phase of ultrashort optical pulses. *Opt. Commun.*, 113:79–84, 1994.

[27] D. Marcuse. Pulse distortion in single-mode fibers. *Appl. Opt.*, 19(10):1653–1660, 1980.

[28] D. Marcuse. Pulse distortion in single-mode fibers. part 2. *Appl. Opt.*, 20(17):2969–2974, 1981.

[29] D. Marcuse. Pulse distortion in single-mode fibers. 3: Chirped pulses. *Appl. Opt.*, 20(20):3573–3579, 1981.

[30] Melles Griot. *Melles Griot Catalog.* 1998.

[31] A. Delgarno and A. E. Kingston. The refractive indices and verdet constants of the inert gases. *Proc. R. Soc. London ser. A*, 259:424–429, 1966.

Appendices

A Propagation equation

To study the behavior of light propagating in any material one have to study Maxwell's equations

$$\nabla \times E = -\frac{\partial B}{\partial t}, \tag{39}$$

$$\nabla \times H = J_f + \frac{\partial D}{\partial t}, \tag{40}$$

$$\nabla \cdot D = \rho_f, \tag{41}$$

$$\nabla \cdot B = 0. \tag{42}$$

The flux densities D and B is due to the medias response to E and H and can be rewritten as:

$$D = \varepsilon_o E + P, \tag{43}$$

$$B = \mu_o H + M, \tag{44}$$

for a non-magnetic media $M = 0$. Using equations (40), (43) and (44) equation (39) can be rewritten in the following way by taking the curl of equation (39):

$$\begin{aligned} \nabla \times \nabla \times E &= \nabla \times \left(-\frac{\partial B}{\partial t}\right) = -\frac{\partial}{\partial t}(\nabla \times B) = \{M = 0\} = -\mu_o \frac{\partial}{\partial t}(\nabla \times H) = \\ \{J_f = 0\} &= -\mu_o \frac{\partial}{\partial t}\left(\frac{\partial D}{\partial t}\right) = -\mu_o \frac{\partial^2}{\partial t^2}(\varepsilon E + P) = \left\{\mu_o \varepsilon_o = \frac{1}{c^2}\right\} = \\ &= -\frac{1}{c^2}\frac{\partial^2 E}{\partial t^2} - \mu_o \frac{\partial^2 P}{\partial t^2} \end{aligned} \tag{45}$$

and using the fact that

$$\nabla \times \nabla \times E = \nabla(\nabla \cdot E) - \nabla^2 E. \tag{46}$$

In a media without charge density, $\rho_f = 0$, (46) can be written as:

$$\nabla \times \nabla \times E = -\nabla^2 E, \tag{47}$$

resulting in

$$\nabla^2 E = \frac{1}{c^2}\frac{\partial^2 E}{\partial t^2} + \mu_o \frac{\partial^2 P}{\partial t^2}. \tag{48}$$

This equation is known as the wave equation and to know the behavior of the light it has to be solved. This is, however, not a very easy task, which involves a lot of quantum mechanics. In the case of a pulse propagating through a capillary some approximations

are possible to make that simplifies matter. One such approximation is that only the nonlinear effects governed by $\chi^{(3)}$ is included, why the polarization can be written as:

$$P(r,t) = P_L(r,t) + P_{NL}(r,t), \tag{49}$$

where P_L is the linear part and P_{NL} is the non-linear part. The wave equation can now be rewritten as:

$$\nabla^2 E - \frac{1}{c^2}\frac{\partial^2 E}{\partial t^2} = \mu_o \frac{\partial^2 P_L}{\partial t^2} + \mu_o \frac{\partial^2 P_{NL}}{\partial t^2}. \tag{50}$$

The next approximation is to study the slowly varying amplitude of the envelope instead of the electric field. This approximation holds as long as the pulses are significantly longer then an optical cycle, i.e. pulses longer than around 10 fs if the wavelength is in the visible region [12]. If the slowly varying envelope is separated from the rapidly changing parts, the electric field and the polarization components can be written as:

$$E(r,t) = \frac{1}{2}\hat{x}\left[\overline{E}(r,t)\exp(-i\omega_o t) + c.c.\right], \tag{51}$$

$$P_L(r,t) = \frac{1}{2}\hat{x}\left[\overline{P}_L(r,t)\exp(-i\omega_o t) + c.c.\right], \tag{52}$$

$$P_{NL}(r,t) = \frac{1}{2}\hat{x}\left[\overline{P}_{NL}(r,t)\exp(-i\omega_o t) + c.c.\right], \tag{53}$$

where c.c. stands for complex conjugate. The non-linear part of the polarization is often small compared to the linear parts so that it can be considered as a pertubation. According to [12] it possible to show that the refractive index is intensity dependent and can be written as:

$$\overline{n}(\omega) = n(\omega) + n_2\left|\overline{E}\right|^2, \tag{54}$$

where the non-linear part, n_2, can be shown to be

$$n_2 = \frac{3}{8n}\chi^{(3)}_{xxxx}. \tag{55}$$

Another parameter that has to be part of the equation is the wave-number, $\beta = \frac{2\pi}{\lambda}$. This parameter depends on the frequency and to simplify matter it is expanded in a Taylor series centered around the central frequency ω_o

$$\beta(\omega) = \beta_o + (\omega-\omega_o)\beta_1 + \frac{1}{2}(\omega-\omega_o)^2\beta_2 + \frac{1}{6}(\omega-\omega_o)\beta_3 + ... \tag{56}$$

where

$$\beta_n = \left(\frac{d^n\beta}{d\omega^n}\right)_{\omega=\omega_o}. \tag{57}$$

After some manipulations the wave equation can be rewritten as:

$$\frac{\partial A}{\partial z} + \beta_1\frac{\partial A}{\partial t} + \frac{i}{2}\beta_2\frac{\partial^2 A}{\partial t^2} + \frac{\alpha}{2}A = i\gamma|A|^2 A, \tag{58}$$

where A is the slowly varying envelope of the pulse and γ is known as the nonlinearity coefficient and is defined as:

$$\gamma = \frac{n_2 \omega_o}{c A_{eff}} \tag{59}$$

and A_{eff} is given by (34).

Since the pulses that are studied in the present work are very short some of the approximations made are not strictly valid and a few more terms are needed in the wave equation. When these terms are added, the frame of reference is also changed to a frame moving along with the pulse

$$T = t - \frac{z}{v_g} = t - \beta_1 z. \tag{60}$$

This finally gives a wave-equation valid for pulses down to ~ 10 fs, [12]

$$\frac{\partial A}{\partial z} + \frac{\alpha}{2} A + \frac{i}{2}\beta_2 \frac{\partial^2 A}{\partial T^2} - \frac{1}{6}\beta_3 \frac{\partial^3 A}{\partial T^3} = i\gamma \left[|A|^2 A + \frac{2i}{\omega_o} \frac{\partial}{\partial T} \left(|A|^2 A \right) - T_R A \frac{\partial |A|^2}{\partial T} \right]. \tag{61}$$

This equation is also known as the generalized nonlinear Schrödinger equation.

For inert gases the response time T_R is very fast (~ 5 fs) and can therefore be neglected if the time duration of the laser pulses are much longer than this. The time scale and the slowly varying envelope can be normalized in the following way:

$$\tau = \frac{T}{T_o}, \tag{62}$$

$$A(z,\tau) = \sqrt{P_o} \exp\left(-\frac{\alpha z}{2} \right) U(z,\tau). \tag{63}$$

Using this and rearranging the terms in equation (61) results in:

$$i\frac{\partial U}{\partial z} = \frac{sgn(\beta_2)}{2L_D} \frac{\partial^2 U}{\partial \tau^2} + i\frac{sgn(\beta_3)}{6L'_D} \frac{\partial^3 U}{\partial \tau^3} - \frac{e^{-\alpha z}}{L_{NL}} \left[|U|^2 U + is \frac{\partial}{\partial \tau} \left(|U|^2 U \right) \right], \tag{64}$$

where:

$$L_D = \frac{T_o^2}{sgn(\beta_2)}, \tag{65}$$

$$L'_D = \frac{T_o^3}{sgn(\beta_3)}, \tag{66}$$

$$L_{NL} = \frac{1}{\gamma P_o}, \tag{67}$$

$$s = \frac{2}{\omega_o T_o}. \tag{68}$$

B Split-step Fourier method

When one wants to know the behavior of a pulse propagating in a media equation (61) has to be solved. This equation is not possible to solve analytically except in a few special cases. It is therefore necessary to solve it numerically, and one way to do it is to use the Split-step Fourier method. The idea behind the Split-step Fourier method is to treat the operators that accounts for the dispersion and absorption and the operators for the nonlinearities separately. Equation(61) can now be written as

$$\frac{\partial A}{\partial z} = \left(\widehat{D} + \widehat{N}\right) A, \tag{69}$$

where:

$$\begin{aligned} \widehat{D} &= -\frac{i}{2}\beta_2 \frac{\partial^2}{\partial T^2} + \frac{1}{6}\beta_3 \frac{\partial^3}{\partial T^3} - \frac{\alpha}{2}, \\ \widehat{N} &= i\gamma \left[|A|^2 + \frac{2i}{\omega_o A} \frac{\partial}{\partial T} \left(|A|^2 A \right) - T_R \frac{\partial |A|^2}{\partial T} \right]. \end{aligned} \tag{70}$$

If the two operators are treated as if they were independent equation (69) can be solved in two steps. The first step is to solve the equation if the nonlinearities acts alone, $\widehat{D} = 0$ and the second step is to solve the equation when dispersion acts alone, $\widehat{N} = 0$. The solution is then given by:

$$A(z+h,T) \simeq \exp\left(h\widehat{D}\right) \exp\left(h\widehat{N}\right) A(z,T). \tag{71}$$

The exponential operator $\exp\left(h\widehat{D}\right)$ is calculated in the Fourier domain:

$$\exp\left(h\widehat{D}\right) B(z,T) = \left\{ F^{-1} \exp\left[h\widehat{D}(i\omega) \right] F \right\} B(z,T),$$

$\widehat{D}(i\omega)$ is obtained by replacing all the $\frac{\partial}{\partial T}$ by $i\omega$ in (70)

$$\widehat{D}(i\omega) = \frac{i}{2}\beta_2\omega^2 - \frac{i}{6}\beta_3\omega^3 - \frac{\alpha}{2}.$$

It can be shown that this method is accurate to the second order in the step size h. To improve the method it has to be taken into account that $\widehat{N}$ varies across h, until now we have just added the nonlinearities at the boundaries of each section, one way to do this is to rewrite equation (71) as:

$$A(z+h,T) \simeq \exp\left(\frac{h}{2}\widehat{D}\right) \exp\left(\int_z^{z+h} \widehat{N}(z')\, dz' \right) \exp\left(\frac{h}{2}\widehat{D}\right) A(z,T).$$

This is called the symmetrized split-step Fourier method. The integral accounts for the z-dependence of the nonlinearities. It can be shown that this method is accurate to the

third order of the step size h. This expression is however more complicated to calculate, even if we use a very rough estimate of the integral (the trapezoidal rule)

$$\int_z^{z+h} \widehat{N}(z')\,dz' \simeq \frac{h}{2}\left[\widehat{N}(z) + \widehat{N}(z+h)\right],$$

we end up with an expression that we have to iterate. However, since the accuracy is higher we can use bigger steps, h, and gain time anyhow. The method can be visualized in the following way: think of the capillary as divided in equispaced segments (separated by h). The pulse propagates the distance $h/2$ only effected by dispersion, then it's multiplied with a term that represents the nonlinear effect over the entire segment and after that it propagates the remaining $h/2$ only effected by dispersion.

The split-step Fourier method is often referred to as the beam-propagation method in the case when diffraction is studied instead of dispersion [12].

C Gaussian beams

The spatial profile of a laser beam along the z-axis can very often be described as Gaussian pulse shape:

$$U(z) \sim \exp\left(-\frac{x^2+y^2}{\omega^2(z)}\right), \tag{72}$$

where $\omega(z)$ is $1/e$ beam radius. A beam with this shape is called a Gaussian beam. Even when the shape is not exactly Gaussian, it is often assumed to be Gaussian since it makes the mathematics easier. The shape of a Gaussian beam is not changed when the beam is focused, but remains Gaussian (the beam radius $\omega(z)$ will of course change). For Gaussian beams a few useful formulas can be derived. The intensity is given by:

$$I = I_o \exp\left(-2\frac{x^2+y^2}{\omega^2(z)}\right), \tag{73}$$

where I_o is the peak intensity of the pulse. When a Gaussian beam is focused, geometrical optics is not valid and the beam size in the focal point is given by:

$$\omega_o = \frac{f\lambda}{\pi\omega}, \tag{74}$$

where ω_o is the beam radius in the focal plane, f is the focal length of the focusing element, λ is the wavelength and ω is the beam radius when the beam enters the focusing element. It is often good to know for how long the beam will be close to its minimum size and the parameter controlling this is known as the Rayleigh distance, z_R

$$z_R = \frac{\pi\omega_o^2}{\lambda}. \tag{75}$$

This is the distance from the focal plane to the point where the beam diameter has increased by a factor $\sqrt{2}$. The length of the focus is often referred to as the confocal parameter $b = 2 \cdot z_R$, since the beam within this length is smaller then $\omega_o\sqrt{2}$. In the focal plane the wave fronts are plane but outside they will be curved. The radius of curvature is given by:

$$R(z) = z + \frac{z_R}{z}, \tag{76}$$

where z is the distance from the focal plane. The size of the beam outside the focal plane is given by:

$$\omega(z) = \omega_o\sqrt{1+\frac{z^2}{z_R^2}}. \tag{77}$$

For large values of z the radius of curvature approaches z and ω increases approximately linearly with z, in this region geometrical optics is approximately valid, [13].

D Propagation in capillaries

To describe a wave, the wave number is often used. In vacuum the wave number is defined as:

$$k = \frac{2\pi}{\lambda}. \tag{78}$$

If the pulses propagate in a media with a refractive index, $n \neq 0$ then the wave number is called β and given by:

$$\beta = n \cdot k = \frac{2\pi n(\lambda)}{\lambda}, \tag{79}$$

where $n(\lambda)$ is the refractive index as a function of the wavelength, λ. The group velocity, v_g and the group velocity dispersion, GVD, includes the derivative and the second derivative of the wave number with respect to the angular frequency, ω. The following relations are useful to the calculations:

$$\begin{aligned} \omega &= \frac{2\pi c}{\lambda}, \\ \partial\omega &= -\frac{2\pi c}{\lambda^2}\partial\lambda, \\ \frac{\partial\beta}{\partial\omega} &= -\frac{\lambda^2}{2\pi c}\frac{\partial\beta}{\partial\lambda}, \end{aligned} \tag{80}$$

which gives:

$$\begin{aligned} \beta_1 &= \frac{\partial\beta}{\partial\omega} = \frac{1}{c}\left(n - \lambda\frac{\partial n}{\partial\lambda}\right), \\ \beta_2 &= \frac{\partial^2\beta}{\partial\omega^2} = \frac{\lambda^3}{2\pi c^2}\frac{\partial^2 n}{\partial\lambda^2}, \\ \beta_3 &= \frac{\partial^3\beta}{\partial\omega^3} = -\frac{\lambda^2}{(2\pi)^2 c^3}\left(3\lambda^2\frac{\partial^2 n}{\partial\lambda^2} + \lambda^3\frac{\partial^3 n}{\partial\lambda^3}\right). \end{aligned} \tag{81}$$

These expressions are also given by [27, 28, 29]. When the pulse propagates in a capillary the wave number will be effected and instead given by:

$$\beta = \frac{2\pi}{\lambda}\left[1 - \frac{1}{2}\left(\frac{2.405 \cdot \lambda}{2\pi a}\right)\right], \tag{82}$$

according to [8], a is the radius of the capillary and $2.405 = u_{11}$. The first part is the same as before if the pulse propagates in vacuum and the second part is the effect due to the capillary. If the pulse propagates in a medium the wave number will instead be given by:

$$\beta = \frac{2\pi}{\lambda}\left[n(\lambda) - \frac{1}{2}\left(\frac{2.405 \cdot \lambda}{2\pi a}\right)\right]. \tag{83}$$

This means that the refractive index will affect the group velocity and dispersion the same way as without the capillary, but there will be contributions due to the capillary.

$$\beta_{1,capillary} = \frac{\lambda^2}{2c}\left(\frac{2.405}{2\pi a}\right)^2 \tag{84}$$

$$\beta_{2,capillary} = -\frac{\lambda^3}{2\pi c^2}\left(\frac{2.405}{2\pi a}\right)^2 \quad (85)$$

$$\beta_{3,capillary} = \frac{3\lambda^4}{(2\pi)^2 c^3}\left(\frac{2.405}{2\pi a}\right)^2 \quad (86)$$

The most interesting feature of this is that the capillary contributes with negative GVD. This contribution is rapidly decreasing with increasing radius, a.

D.1 The refractive index

The refractive index is dependent on the wavelength and the dependence is for solid material given by:

$$n = \sqrt{1 + \frac{B_1\lambda^2}{\lambda^2 - C_1} + \frac{B_2\lambda^2}{\lambda^2 - C_2} + \frac{B_3\lambda^2}{\lambda^2 - C_3}}, \quad (87)$$

where λ is given in μm. This formula has an accuracy of 10^{-5} in the wavelength region $365\ nm < \lambda < 2300\ nm$. For some ordinary optics material the constants are given by:

	FS	$BK7$	$SF11$
B_1	0.6961663	1.03961212	1.73848403
B_2	0.4079426	0.231792344	0.311168974
B_3	0.8974794	1.01046945	1.17490871
C_1	$(0.0684043)^2$	$6.00069867 \cdot 10^{-3}$	$1.36068604 \cdot 10^{-2}$
C_2	$(0.1162414)^2$	$2.00179144 \cdot 10^{-2}$	$6.15960463 \cdot 10^{-2}$
C_3	$(9.896161)^2$	$1.03560653 \cdot 10^2$	$1.21922711 \cdot 10^2$

According to [30].

According to [31] the refractive index of Ar and Kr are given by:

$$n_{Ar}^2 - 1 = 5.547 \cdot 10^{-4}\left(1 + \frac{5.15 \cdot 10^5}{\lambda^2} + \frac{4.19 \cdot 10^{11}}{\lambda^4} + \frac{4.09 \cdot 10^{17}}{\lambda^6} + \frac{4.32 \cdot 10^{23}}{\lambda^8} + ...\right),$$

$$n_{Kr}^2 - 1 = 8.377 \cdot 10^{-4}\left(1 + \frac{6.70 \cdot 10^5}{\lambda^2} + \frac{8.84 \cdot 10^{11}}{\lambda^4} + \frac{1.49 \cdot 10^{18}}{\lambda^6} + \frac{2.74 \cdot 10^{24}}{\lambda^8} + ...\right).$$

Here the wavelength is measured in Å.

E Autocorrelators

Today there is no electronic detector capable of measuring the time duration of ultrashort femtosecond laser pulses[18]. To time resolve such short pulses nonlinear optical techniques must be used. These techniques takes advantage of the fact that the speed of light is very high and the idea is to convert the measurement from the time domain into the space domain. A light pulse covers a significant distance even during a very short period of time. In 10 fs a light pulse travels 3 μm. This is a distance which can be easily measured but there are no detector capable of directly measure 10 fs.

The most common method is known as the second harmonic autocorrelator technique. This autocorrelator can be designed either for multi shot or single shot operation. The multi shot autocorrelator uses several laser pulses to measure the time duration while the single shot only uses one laser pulse.

E.1 Multi shot autocorrelator

The design of the multi shot autocorrelator is depicted in Figure 29. The optical pulse is divided into two pulses, one of which passes through a variable delay line. The delay is controlled using a translation stage. Both pulses are then recombined in a frequency doubling crystal[19]. If the crystal is properly oriented for phase matching conditions[20] second harmonic light with the frequency 2ω is created in the direction of propagation of each beam. If the pulses in the two beams overlap spatially and temporally second harmonic light will also be created along the bisector of the two beams. The frequency doubled light at the bisector is the signal, measured with a slow integrating photodetector. The detected signal is proportional to the function:

$$S(\tau) \sim \int_{-\infty}^{\infty} I(t)\, I(t-\tau)\, dt. \tag{88}$$

This function is known as the intensity autocorrelation function. By moving the translation stage, the value of τ is altered at the same time as the signal is measured. The signal $S(\tau)$ can then be used to calculate the time duration of the laser pulses. The FWHM of $S(\tau)$, τ_{ac}, is proportional to the FWHM time duration of the pulses, τ_p

$$\tau_{ac} = a \cdot \tau_p. \tag{89}$$

The value of the constant a depends on the actual shape of the pulses. If a Gaussian pulse shape is assumed $a = 1.414$ and if the shape is assumed to be $sech^2$ $a = 1.543$.

[18]The electronic detector with best resolution today is streak cameras which can resolve sub picosecond pulses.

[19]The crystal used in the thesis work was a KDP-crystal.

[20]Phase matching means that both the beams with frequency ω and 2ω propagates with the same velocity inside the crystal. This insure that the energy transfer from the beam with frequency ω to the beam with frequency 2ω always occurs constructively.

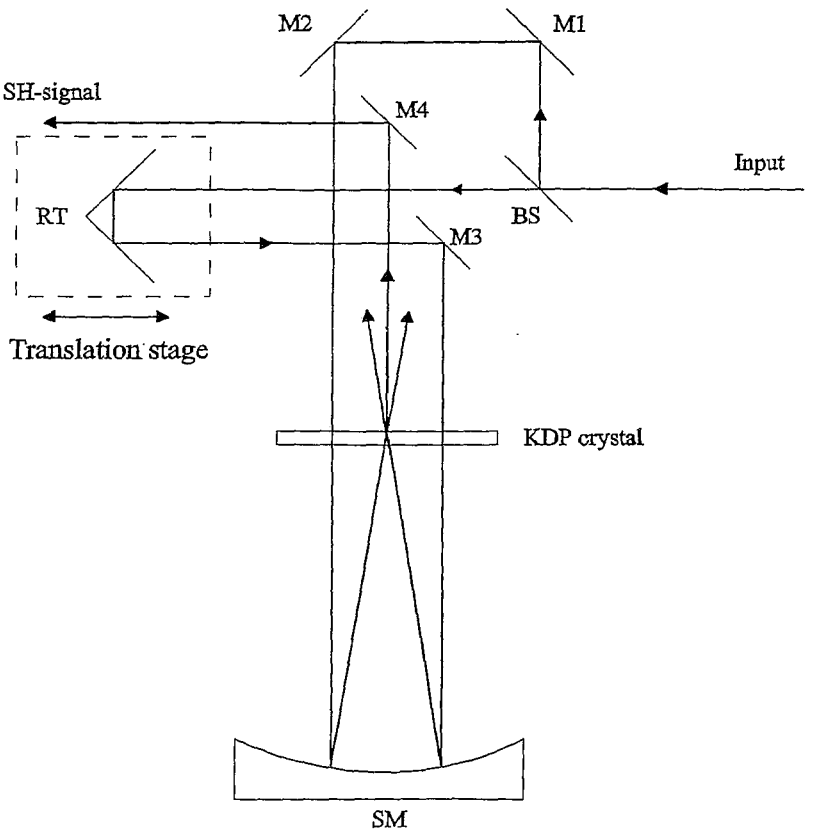

Figure 29. The design of a multi shot autocorrelator. The input beam is split into two parts by the beam splitter (BS). One of the pulses passes a variable delay line controlled by a translation stage. M1-4 are mirrors used for guiding the beam and RT is a roof-top mirror. The beams are focused into a KDP-crystal using a spherical mirror (SM). The second harmonic signal (SH-signal) is created at the bisector of the two beams when the pulses overlap spatially and temporally and detected using a photo detector.

E.2 Single shot autocorrelator

It is not always convenient to use a multi shot autocorrelator, e.g. when the pulse duration fluctuates on a shot–to–shot basis, or if the repetition rate is too slow. It is then necessary to measure the pulse duration using only one shot. A device that makes this possible is called a single shot autocorrelator. The design of a single shot autocorrelator is depicted in Figure 30.

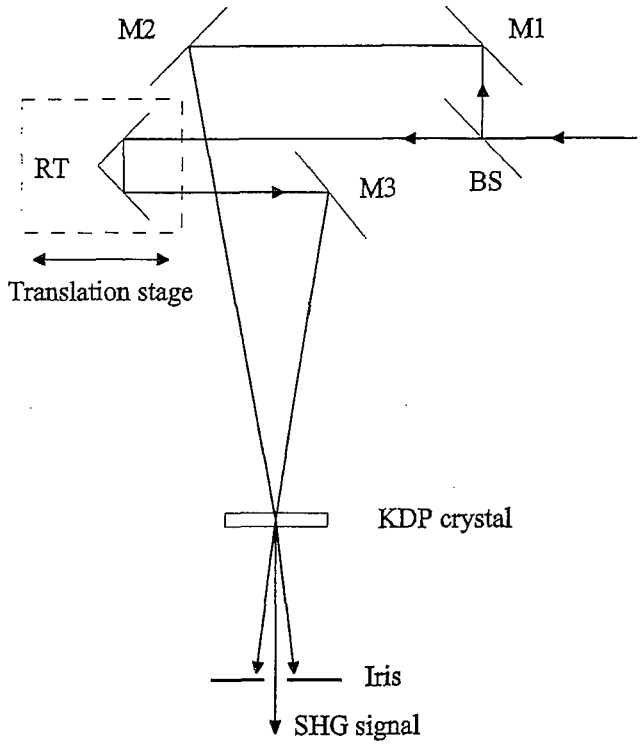

Figure 30. The design of a single shot autocorrelator. The beam is split in two parts by a beam splitter (BS). M1-3 are mirrors used to guide the beams and RT is a roof-top mirror placed on a translation stage. The two beams are recombined in a KDP-crystal. When the pulses in the two beams overlap spatially and temporally a second harmonic signal is created at the bisector of the two beams. This signal is measured using a CCD-array. The iris is used to block the second harmonic light created directly by either of the two beams.

As in the multi shot autocorrelator the pulse to be measured is divided in two pulses which are recombined in the frequency doubling crystal, which is arranged for phase matching for the two intersecting beams. The angle between the beams is made small. Provided that the overlap region is much larger than the pulse length, $v_g \tau_p$, the intensity distribution across the second harmonic beam at the bisector corresponds to the intensity autocorrelation function (88). This signal is measured using a CCD-array. To calibrate the single shot autocorrelator one of the beams is delayed using the translation stage.

More information on autocorrelator and different designs can be found in, for example [25] and [11].